A PLACEMENT MODEL FOR MATRIX ACIDIZING OF VERTICALLY EXTENSIVE, MULTILAYER GAS RESERVOIRS

A Thesis

by

MANABU NOZAKI

Submitted to the Office of Graduate Studies of
Texas A&M University
in partial fulfillment of the requirements for the degree of

MASTER OF SCIENCE

August 2008

Major Subject: Petroleum Engineering

A PLACEMENT MODEL FOR MATRIX ACIDIZING OF VERTICALLY EXTENSIVE, MULTILAYER GAS RESERVOIRS

A Thesis

by

MANABU NOZAKI

Submitted to the Office of Graduate Studies of
Texas A&M University
in partial fulfillment of the requirements for the degree of

MASTER OF SCIENCE

Approved by:

Chair of Committee,	A. Daniel Hill
Committee Members,	Christine Ehlig-Economides
	Zhengdong Cheng
Head of Department,	Stephen A. Holditch

August 2008

Major Subject: Petroleum Engineering

ABSTRACT

A Placement Model for Matrix Acidizing of Vertically Extensive, Multilayer Gas Reservoirs. (August 2008)

Manabu Nozaki, B.E., Waseda University

Chair of Advisory Committee: Dr. A. Daniel Hill

Design of matrix acidizing treatments of carbonate formation is still a challenge although extensive research has been done on it. It is necessary to estimate acid distribution along the wellbore. This estimation is very important especially for the case where the reservoir properties vary along the wellbore.

This work provides development and application of an apparent skin factor model which accounts for both damage and mobility difference between acid and gas. Combining this model with a conventional acid placement model, we develop an acid placement model for vertically extensive, multilayer gas reservoirs. A computer program is developed implementing the acid placement model. The program is used to simulate hypothetical examples of acid placement for vertically extensive, multilayer gas reservoirs. This model will improve matrix acidizing for gas reservoirs and enable real-time monitoring of acid stimulation more accurately.

DEDICATION

This thesis is dedicated to my parents,

Matsuhiro and *Yoshiko Nozaki*

ACKNOWLEDGEMENTS

I would like to take this opportunity to express my deepest gratitude and appreciation to my advisor and committee chair, Dr. A. Daniel Hill, for his continuous encouragement and especially for his academic guidance. Also, I would like to thank Dr Ding Zhu and Dr. Hisham Nasr-El-Din for their advice, guidance, and encouragement during the course of this research.

Appreciation is extended to the members of my committee, Dr. Christine Ehlig-Economides and Dr. Zhengdong Cheng for their help.

I also would like thank my colleagues, Maysam Pournik, Weibo Sui, and Xiaoqing Wu for their friendship and help during my graduate study.

Finally, I would like to acknowledge financial support from the Middle East Carbonate Stimulation joint industry project at Texas A&M University. The facilities and resources provided by the Harold Vance Department of Petroleum Engineering of Texas A&M University are gratefully acknowledged.

TABLE OF CONTENTS

Page

LIST OF FIGURES

Page

Page

LIST OF TABLES

Page

1. INTRODUCTION

1.1 Statement of the Problem

Matrix acidizing is a well stimulation technique in which an acid solution is injected into the formation in order to dissolve some of the minerals present, and hence, recover or increase permeability. The acidizing treatment is called a matrix treatment because the acid is injected at pressures below the parting pressure of the formation, so that fractures are not created. The objective is to greatly enhance or recover the permeability near the wellbore, rather than affect a large portion of the reservoir.

Overall acid volumes for the treatment of short intervals in vertical wells tend to be small and good placement efficiency has been obtained in vertical wells. However, for vertically extensive wells, it is hard to stimulate the formation effectively. Some zones cannot be acidized sufficiently. To stimulate the formations effectively, estimating the volume of acid injected into each zone during the treatment is crucial.

Several acid placement models for oil reservoirs have been developed and applied in the field successfully. In those models transient flow or pseudosteady-state flow equation, and Hawkins' formula are used to evaluate the effectiveness of the stimulation. However, when evaluating acidizing in a gas well, the models are not adequate because the mobility (viscosity and relative permeability) difference

---

This thesis follows the style of *SPE* Journal.

between the reservoir fluid (gas) and the injected fluid (acid) mainly affects the damage reduction process. Hence, an model for matrix acidizing in gas wells needs to account for such an effect to evaluate the effectiveness of the treatment.

1.2 Background and Literature Review

Extensive research has been done on modeling acid placement in horizontal wells; however, only limited number of models for vertical wells exists in literature (Hill and Galloway, 1984; Hill and Rossen, 1994) because overall acid volumes for the treatment of short intervals in vertical wells tend to be small and good placement efficiency has been obtained. Even though acid-placement modeling in horizontal wells is more complicated, the same concepts can be applied for vertical wells.

Jones and Davies (1996) presented an acid placement model for horizontal wells. The model was for barefoot completions in sandstone formations, and the simulator used a pseudosteady-state reservoir model. They emphasized the need to include wellbore phenomena.

Using well testing theory, Hill and Zhu (1996) developed the real-time monitoring model for acidizing of single-phase oil reservoirs for the transient reservoir response. The model yielded the damage skin evolution from an inverse injectivity versus superposition time plot. On the basis of their model, Eckerfield et al. (2000) and Mishra et al. (2007) presented an acid-placement model for horizontal wells including an interface tracking model.

Gdanski (2005) described recent advances in carbonate stimulation, stating that zonal coverage of long carbonate sections remains a challenge and most of the acidizing treatments are still designed on the basis of rules of thumb.

Zhu et al. (1998) presented a real-time monitoring model for acidizing of gas wells. In their model they successfully estimated skin evolution during an acid treatment for gas wells, accounting for a big difference of viscosity between acid and gas. On the basis of their model, Fadele et al. (2000) modeled acid treatment for gas reservoirs. However, their model didn't account for wellbore phenomena.

1.3 Objectives of Research

In this study, the effect of mobility difference between gas and acid is evaluated more accurately than the Fadele et al. model (2000) In addition, we account for wellbore phenomena by combining the wellbore flow model and the reservoir outflow model in the same way as Mishra et al. (2007). The model will improve acid treatments design for multilayer gas reservoirs and real-time monitoring.

The presented research project aims to develop an acid placement model for vertically extensive, multilayer gas reservoirs. Following are the basic objectives:

- Analyze linear coreflood data.
- Construct an apparent skin factor model on the basis of the analysis of coreflood data.
- Couple the reservoir outflow model, the wellbore flow model, the interface tracking model, and the apparent skin factor model.

- Develop a computer program.
- Apply the computer program to hypothetical data and study the results.

1.4 Outline of the Thesis

In section 2 we analyze Shukla's linear coreflood experimental data (2002), and show the effect of mobility difference between gas and acid.

In section 3 we present the formulation of the various model equations: wellbore flow model, reservoir outflow model, fluid interface tracking model, wormholing model, apparent skin factor model, and mechanical skin effect. The model couples several processes together. Each process is described separately in this section.

In section 4 we show a method to solve the model equations presented in section 3. Also the details of a computer program developed are presented.

In section 5 we apply the computer program to hypothetical data. We study both one-layer case and multilayer case.

In section 6, the new developments from this work and their practical applicability are summarized. Potential future research works are also suggested.

2. LINEAR COREFLOOD DATA ANALYSIS

2.1 Introduction

When carbonates are acidized using hydrochloric acid, the dissolution of rock matrix is not uniform as in sandstone acidizing. Instead, highly conductive flow channels known as wormholes result due to non-uniform dissolution. Thus, this highly selective pattern of dissolution dissolves certain parts of the medium creating infinitely permeable channels whereas other parts remain unaffected.

The propagation of wormholes during carbonate acidizing has been studied extensively, both experimentally and theoretically. A key finding of the experimental studies has been that if a given acid is pumped at a constant rate into a liquid saturated core maintained under confining pressure at a certain temperature within a core holder, then the differential pressure across the core declines mostly linearly with time (**Fig. 2.1**).

However, Shukla (2002) showed that this is not always true for acidizing in a gas saturated core. He carried out 19 experiments. In the five experiments the differential pressure built up until it reached a maximum differential pressure, and dropped rapidly (**Fig. 2.2**). This increase of differential pressure could be explained in terms of relative permeability and viscosity difference between gas and acid.

We analyze Shukla's linear coreflood data by applying Darcy's law along the core length.

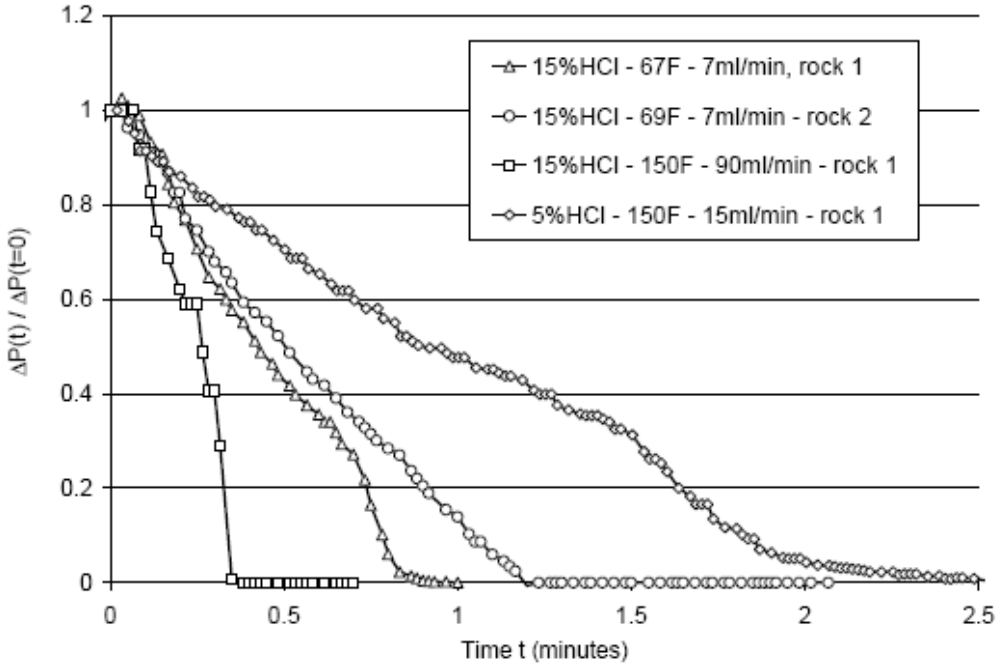

Fig. 2.1—Typical curves of pressure drop observed with HCl in limestone rocks (from Tardy et al., 2007).

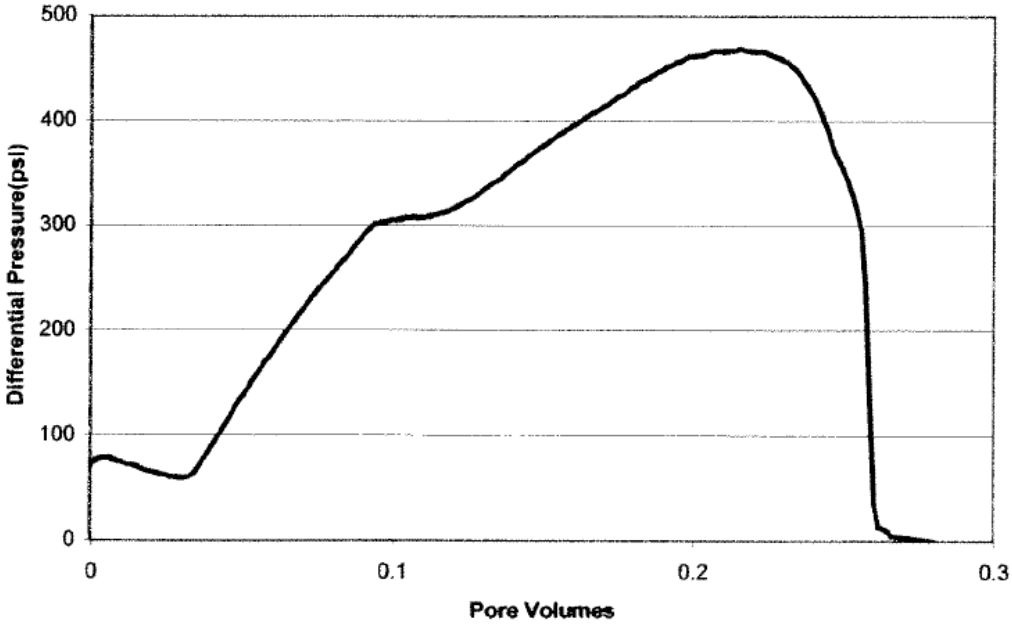

Fig. 2.2—Differential pressure versus pore volumes in a gas saturated core (from Shukla, 2002).

2.2 Experiment Description

The layout of Shukla's experimental apparatus is shown in **Fig. 2.3**. In the experiments, first gas was injected into a liquid saturated core until the core was at residual water saturation. Then acid was injected until wormhole broke through. Acidizing condition such as temperature, injection rate and gas injection method were varied. The permeability response during acidizing was monitored.

The cores were 6" long and 1" diameter cores fabricated from a Texas Cream Chalk rock sample of average permeability of 6.5 md and average porosity of 28 %.

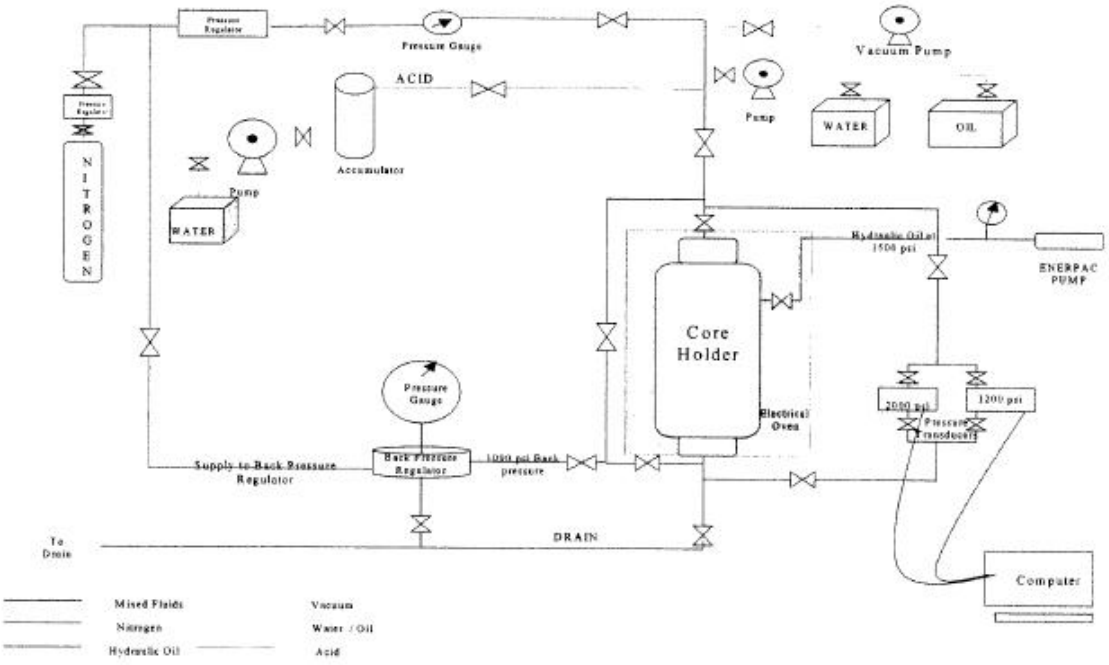

Fig. 2.3—Experiment setup (from Shukla, 2002).

2.3 Data Analysis

During acidizing, we have the following three potential zones (**Fig. 2.4**):

I. A zone where wormholes are created and pressure drop is negligible.

II. A zone which is invaded by spent acid.

III. A zone which is filled with an original fluid.

Each zone has different mobility. Using Darcy's law, the total pressure drop is given by

$$\Delta p = \frac{q\mu_{\text{acid}}(L_{\text{spent}} - L_{\text{wh}})}{kk^{\circ}_{\text{ra}}A_{\text{eff}}} + \frac{q\mu_{\text{gas}}(L_{\text{core}} - L_{\text{spent}})}{kk^{\circ}_{\text{rg}}A_{\text{eff}}}, \quad \text{..... (2.1)}$$

where Δp is differential pressure along the core, q is injection rate, μ_{acid} is acid viscosity, L_{spent} is length of spent acid penetration, L_{wh} is length of wormhole penetration, k is absolute permeability, k°_{ra} is endpoint relative permeability to acid, μ_{gas} is gas viscosity, L_{core} is core length, k°_{rg} is endpoint relative permeability to gas, and A_{eff} is effective cross-sectional area.

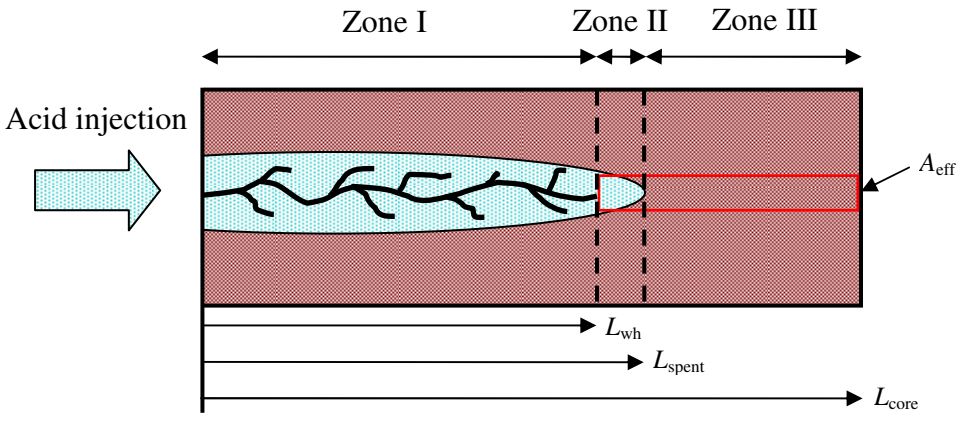

Fig. 2.4—Displacement pattern in a gas saturated core during acidizing.

When acidizing in a liquid saturated core, mobility difference between acid and original fluid is small. Hence the two terms in Eq. 2.1 can be one term. In addition, the length of zone II in a liquid saturated core could be smaller than that in a gas saturated core. According to Shukla (2002), the wormhole in the gas saturated core was observed to have less branching than that in the liquid saturated core. Therefore the first term could be negligible in a liquid saturated core.

Assuming that both L_{wh} and L_{spent} increase with time linearly, then the total pressure drop is at its maximum when the front of spent acid gets to the outlet of the core. Then,

$$\Delta p_{max} = \frac{q\mu_{acid}(L_{core} - L^*_{wh})}{kk^\circ_{ra}A_{eff}} \quad \text{..... (2.2)}$$

Using Eqs. 2.1 and 2.2, $\Delta p / \Delta p_{max}$ is given by

$$\frac{\Delta p}{\Delta p_{max}} = \frac{L_{spent} - L_{wh}}{L_{core} - L^*_{wh}} + \frac{\mu_{gas}k^\circ_{ra}(L_{core} - L_{spent})}{\mu_{acid}k^\circ_{rg}(L_{core} - L^*_{wh})} \quad \text{..... (2.3)}$$

Using Eq. 2.3, we analyze the linear coreflood data. We define the velocity of the spent acid front in ft/PV, α_{spent}, and velocity of wormhole growth in ft/PV, α_{wh}, as follows:

$$L_{spent} = \alpha_{spent} PV, \quad \text{..... (2.4)}$$

and

$$L_{wh} = \alpha_{wh} PV. \quad \text{..... (2.5)}$$

Assuming that α_{spent} and α_{wh} are constant, then they are calculated by

$$\alpha_{spent} = \frac{L_{core}}{PV_{bt,spent}}, \quad \text{..... (2.6)}$$

and

$$\alpha_{wh} = \frac{L_{core}}{PV_{bt,wh}} \quad \text{..... (2.7)}$$

Using Eqs.2.4 through 2.7 and properties presented in **Table 2.1**, we analyze Shukla's experiments 16, 17, 22, 30, and 31 (**Table 2.2**). **Figs.2.5 (a)** through **(e)** show the results. A good match is not obtained especially for the first part where spent acid does not break through. In this calculation, the length of zone II might be overestimated.

Next, we separate the curves into two parts, and we use *Microsoft Excel Solver* to get a better match for each part. The results are presented in **Figs. 2.6 (a)** through **(e)**. These results show that α_{spent} and α_{wh} of the first part do not differ so much. This means even if the length of zone II is very short, there is such a big pressure drop in zone II that the pressure drop in zone II dominates the total differential pressure. As to the second part, α_{wh} are very small values. This might be reasonable since according to the Wood's metal castings of Shukla' experimental results the wormhole near the outlet was relatively denser than other part of the wormhole. This may be an "end effect" in a gas saturated case.

Table 2.1—Gas and acid properties of coreflood experiment.	
Nitrogen viscosity, cp	0.00201
Endpoint relative permeability to nitrogen	0.9
Acid viscosity, cp	0.826
Endpoint relative permeability to acid	0.5

Table 2.2—Experimental data (from Shukla, 2002).

Experiment No.	Temperature, °C	Injection rate, lm/min	Acid PV_{bt}
16	50	4.12	0.21
17	50	5.8	0.20
22	50	1.5	1.5
30	50	1.83	1.83
31	50	2.7	2.7

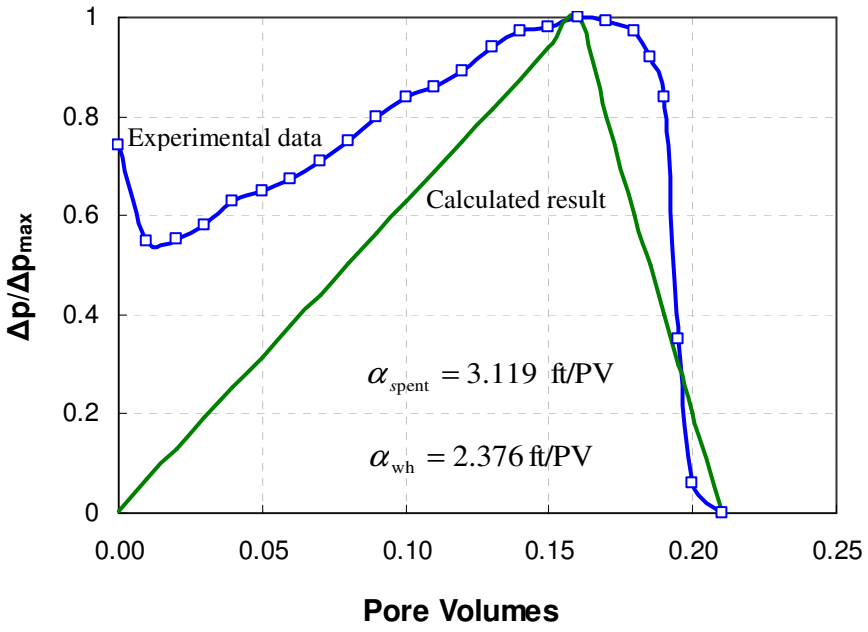

Fig. 2.5 (a)—Data fit in experiment 16 (from Shukla, 2002).

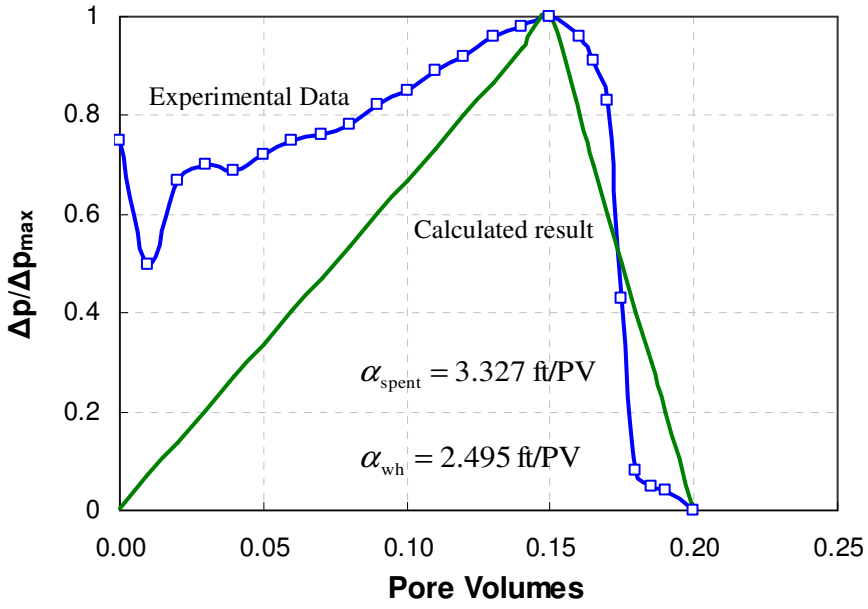

Fig. 2.5 (b)—Data fit in experiment 17 (from Shukla, 2002).

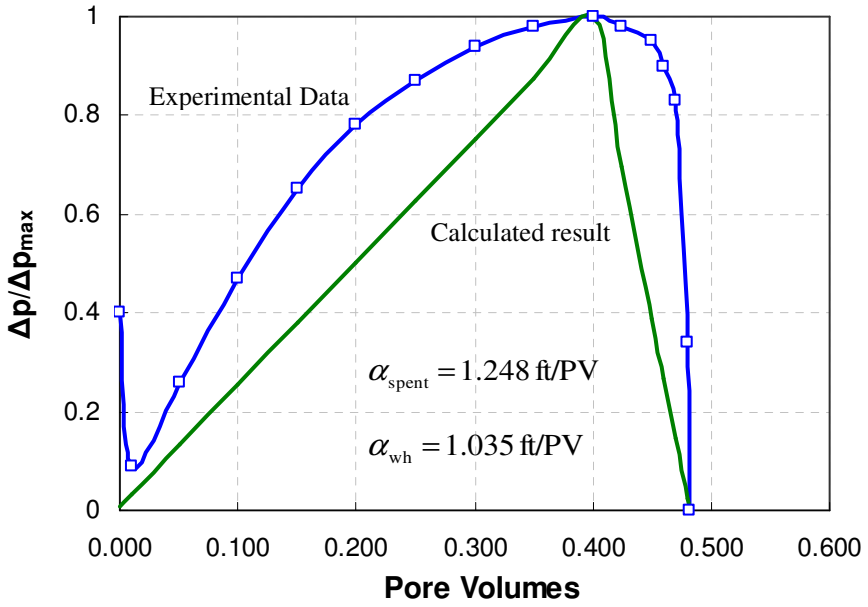

Fig. 2.5 (c)—Data fit in experiment 22 (from Shukla, 2002).

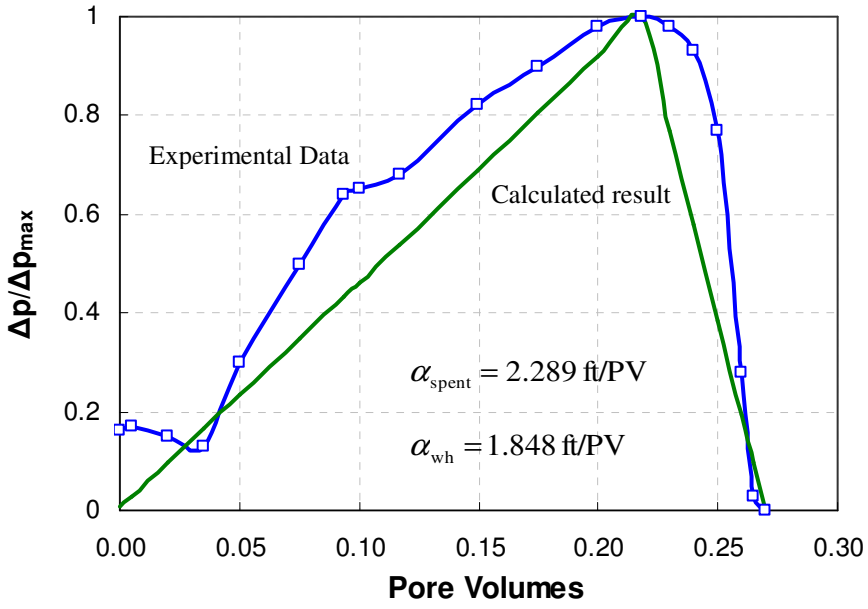

Fig. 2.5 (d)—Data fit in experiment 30 (from Shukla, 2002).

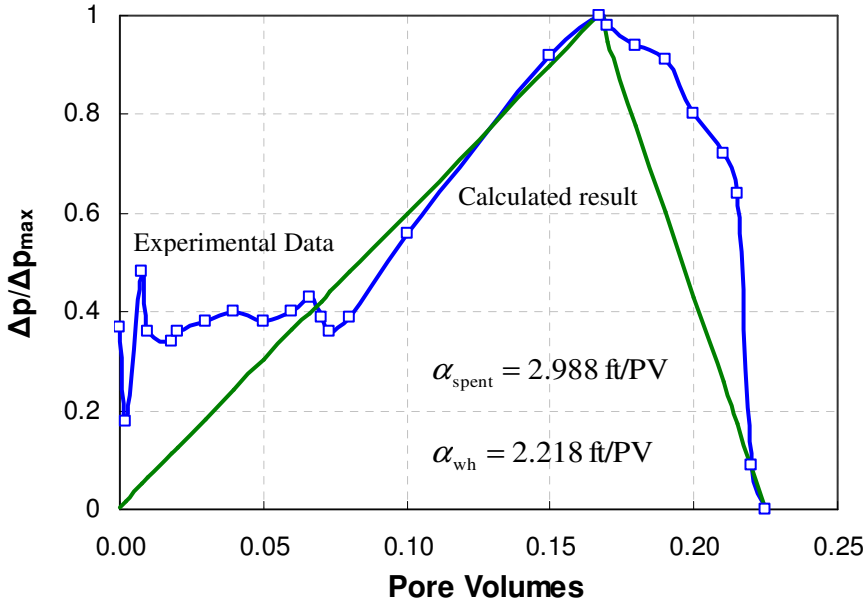

Fig. 2.5 (e)—Data fit in experiment 31 (from Shukla, 2002).

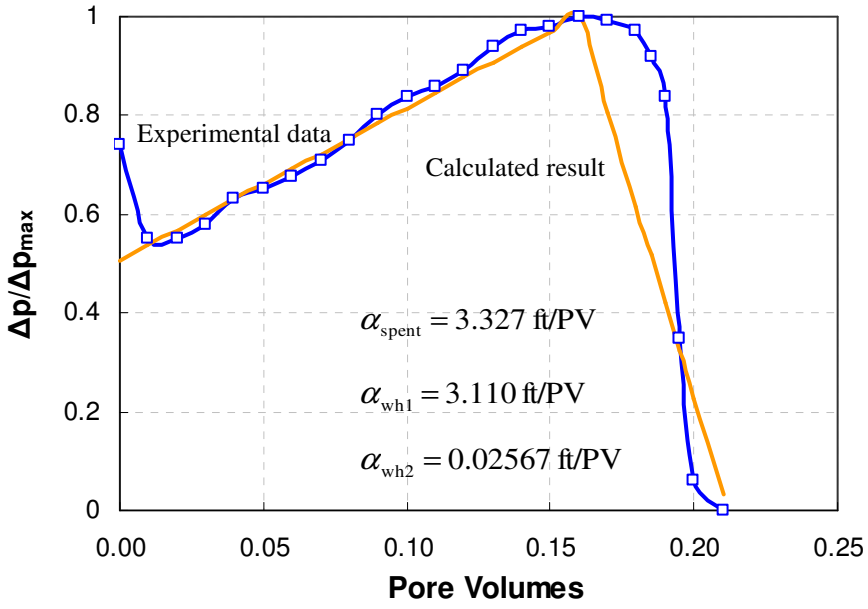

Fig. 2.6 (a)—Data fit in experiment 16 (from Shukla, 2002).

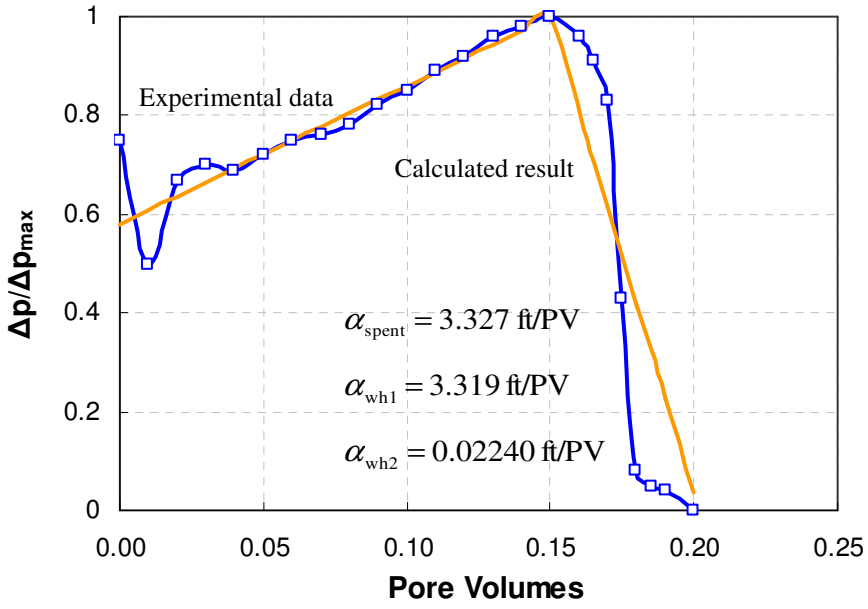

Fig. 2.6 (b)—Data fit in experiment 17 (from Shukla, 2002).

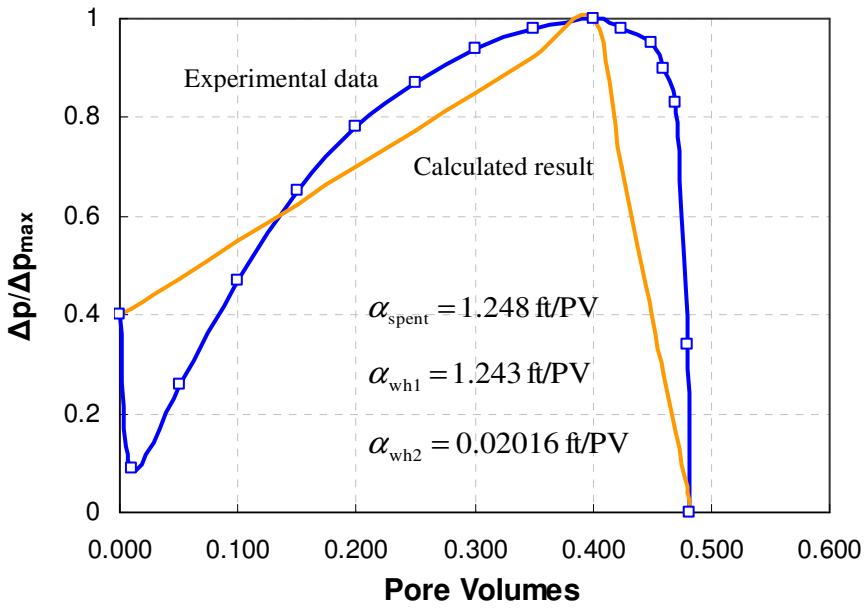

Fig. 2.6 (c)—Data fit in experiment 22 (from Shukla, 2002).

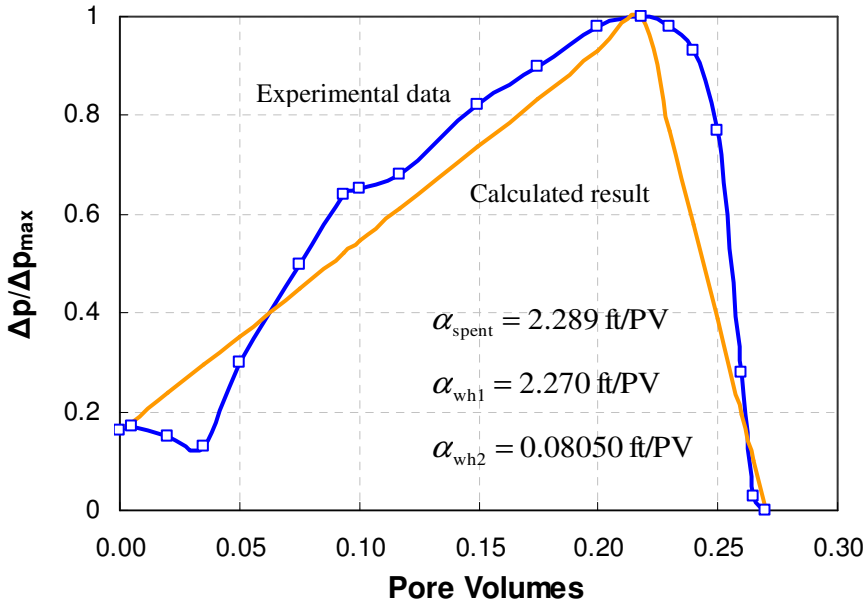

Fig. 2.6 (d)—Data fit in experiment 30 (from Shukla, 2002).

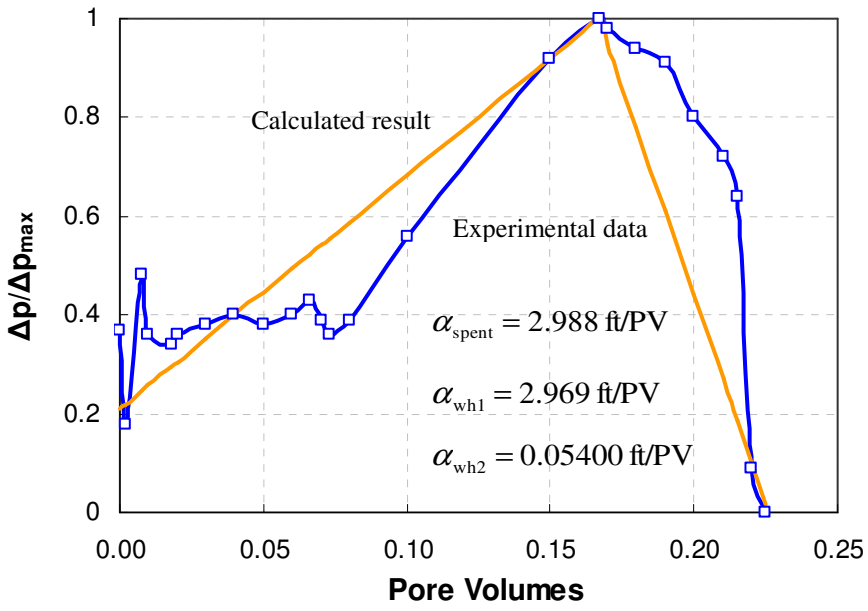

Fig. 2.6 (e)—Data fit in experiment 31 (from Shukla, 2002).

2.4 Section Summary

A good match is obtained by using Eq. 2.1. The result shows that mobility difference can cause a big differential pressure in spent acid zone. Hence if length of spent acid zone (= $L_{spent} - L_{wh}$) is long enough, then mobility difference in the zone is negligible.

3. ACID PLACEMENT MODEL IN GAS WELLS

3.1 Introduction

In this section, an acidizing placement model for gas wells is presented. In a typical matrix acidizing process, acid is injected into the formation through production tubing, coiled tubing, or drill pipe. The acid flows into the formation and creates a few large channels, called wormholes. This enhances the productivity of a well. A critical factor to the success of a matrix acidizing treatment is proper placement of the acid so that all of the productive intervals are contacted by sufficient volumes of acid. If the reservoir properties such as permeability vary significantly, then the acid will tend to flow primarily into the higher-permeability zones, leaving lower-permeability zones virtually untreated. The longer the target zone is, the more difficult it is to stimulate all zones efficiently.

As we discussed in the previous section, it is needed to evaluate the effect of mobility difference between acid and gas during acidizing in gas wells. To account for this effect, we introduce a new apparent skin factor model. This model also accounts for damage reduction at the same time. This model enables us to estimate the volume of acid injected more accurately than the previous model.

To simulate the acidizing process, an acid placement model includes a wellbore model which handles the pressure drop and material balance in the wellbore; an interface tracking model to predict the movement of interfaces between different fluids in the

wellbore; a transient reservoir flow model; and an apparent skin factor model. Each model is discussed separately.

3.2 Wellbore Flow Model

The wellbore flow model is developed on the basis of wellbore material balance and wellbore pressure drop calculations. The fluids injected during the acid injection process are mostly incompressible so single phase incompressible flow in the wellbore is assumed in these equations.

3.2.1 Wellbore Material Balance

Fig. 3.1 shows a schematic of a slanted wellbore during an acid injection process. Single phase (liquid) flow through a reservoir in a fully penetrating deviated well is considered. Apparently the reservoir flow in the slanted well is not perpendicular to the wellbore. This effect can be accounted for by slant skin effect (discussed later). p_w is wellbore pressure at any point in the wellbore, q_w is the flow rate in the wellbore, and q_{sR} is specific reservoir outflow i.e. per unit thickness. The flow rate changes along the wellbore due to the fluid flow into the reservoir. As a result, material balance will give

$$\frac{\partial q_w}{\partial z} = -q_{sR.} \quad \text{..... (3.1)}$$

Eq. 3.1 states that the specific reservoir outflow should be equal to the decrease in wellbore flow rate per unit thickness.

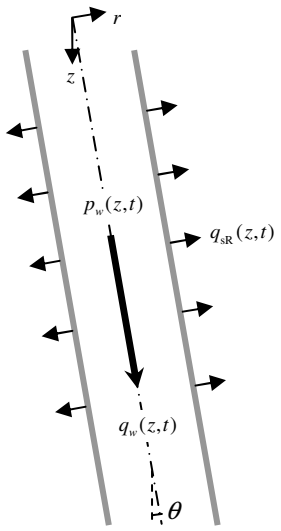

Fig. 3.1—Schematic of a section of a slanted well during an acidizing.

3.2.2 Wellbore Pressure Drop

The pressure drop of single-phase flow in a pipe over distance, *L*, can be obtained by solving the mechanical energy balance equation, which in differential form is

$$\frac{dp}{p}+\frac{udu}{g_c}+\frac{g}{g_c}dz+\frac{2f_f u^2 dL}{g_c D}+dW_s=0 \quad \text{..... (3.2)}$$

If the fluid is incompressible (ρ is constant), and there is no shaft work device in the pipeline, this equation can be readily integrated to yield

$$\Delta p = p_1 - p_2 = \frac{g}{g_c}\rho\Delta z+\frac{\rho}{2g_c}\Delta u^2+\frac{2f_f \rho u^2 L}{g_c D} \quad \text{..... (3.3)}$$

for fluid moving from position 1 to position 2. The three terms on the right-hand side are potential energy, kinetic energy, and frictional contribution to the overall pressure drop, or

$$\Delta p = \Delta p_{PE} + \Delta p_{KE} + \Delta p_{F} \quad \text{..... (3.4)}$$

Generally, there is no change in cross-sectional area of the pipe in the reservoir zone. Hence the pressure drop due to kinetic energy change is zero. Also, the frictional pressure drop is negligible since the pressure drop due to potential energy change dominate the total pressure drop (if gelled or foamed acid is used, this assumption is invalid).

The potential energy pressure drop, Δp_{PE}, is given by

$$\Delta p_{PE} = \frac{g}{g_c} \rho L \cos\theta \quad \text{..... (3.5)}$$

where g is acceleration due to gravity in ft/sec^2, g_c is conversion factor in lb_m-ft/lb_f-sec^2, ρ is density of the fluid in lb_m/ft^3, L is pipe length in ft, and θ is defined as the angle between vertical and the direction of flow. Assuming g/g_c = 1.0 lb_f/lb_m and using fresh water density (ρ = 62.4 lb_m/ft^3), we have

$$\Delta p_{PE} = 0.433 \gamma_a \Delta z \quad \text{..... (3.6)}$$

where γ_a is the specific gravity and $\Delta z = L\cos\theta$.

In the differential form the total pressure drop equation can be written as

$$\frac{\partial p_w}{\partial z} = 0.433 \gamma_a \quad \text{..... (3.7)}$$

3.3 Reservoir Outflow Model

The unsteady-state equation for slightly compressible liquid in a homogenous-acting infinite-acting reservoir is the line-source (Ei-function) solution to the diffusivity equation:

$$p_i - p_w = \frac{162.6qB\mu}{kh}\left[\log\left(\frac{kt}{\phi\mu c_t r_w^2}\right) - 3.23 + 0.869s\right], \quad \text{..... (3.8)}$$

where p_i is initial reservoir pressure in psi and is calculated by $\frac{\partial p_i}{\partial z} = 0.433\gamma_g$, p_w is well pressure in psi, q is flow rate in STB/day, B is formation volume factor in resbbl/STB, μ is viscosity in cp, k is effective permeability in md, t is time in hour, ϕ is porosity in fraction, c_t is total compressibility in psi^{-1}, s is skin factor in dimensionless. This equation can be altered by replacing pressure with real-gas pseudopressure. These transformations account for variations in gas properties with pressure. Accuracy is improved for both semilog and type-curve analysis of gas well tests by replacing pressure with the real-gas pseudopressure function, m(p),

$$m(p) = \frac{\overline{\mu}_g \overline{Z}}{\overline{p}} \int_0^p \frac{p}{\mu_g Z} dp \quad \text{..... (3.9)}$$

For some gases at high pressure (e.g., above 3,000 psia), an adequate approximation is

$$\frac{p}{\mu_g Z} = \text{constant} = \frac{\overline{p}}{\overline{\mu}_g \overline{Z}} \quad \text{..... (3.10)}$$

When this approximation is valid, Eq. 3.8 becomes

$$p_i - p_w = \frac{162.6 q_g \overline{B}_g \overline{\mu}_g}{kh}\left[\log\left(\frac{kt}{\phi \overline{\mu}_g \overline{c}_t r_w^2}\right) - 3.23 + 0.869 s\right] \quad \text{..... (3.11)}$$

This approximation is valid for gas reservoirs because typical gas reservoirs exist in such a deeper depth that pressure is higher than 3,000 psia.

Now we consider gas displacement by acid. The mobility ratio, M, of this two-phase flow is defined as,

$$M = \frac{\lambda_{\text{acid}}}{\lambda_{\text{gas}}} \quad \text{..... (3.12)}$$

where

$$\lambda_j = \frac{k_{rj}}{\mu_j} \quad \text{..... (3.13)}$$

In Eq. 3.13, k_{rj} is the relative permeability of phase *j* and μ is the viscosity of phase j. Generally, mobility of acid is less than that of gas. Hence, M < 1. The fractional flow of the acid is given by

$$f_{\text{acid}} = \frac{1}{1 + \text{M}} \quad \text{..... (3.14)}$$

which is greater than 0.5. Therefore there is no tendency for the gas to be by-passed. Then we have a piston-like displacement with a sharp interface between acid and gas. Hence the gas saturation in the acid zone is critical gas saturation, S_{gc} (gas is immobile). Because of a piston-like displacement, the following equation is valid at the interface:

$$q_g \overline{B}_g = q_a B_a \quad \text{..... (3.15)}$$

where q_a is acid solution flow rate in STB/day and B_a is acid solution formation volume factor in resbbl/STB. In addition, using an apparent skin factor (discussed later) to account for pressure drop in the acid zone, then Eq. 3.11 becomes

$$p_i - p_w = \frac{162.6 q_a B_a \bar{\mu}_g}{kh}\left[\log\left(\frac{kt}{\phi \bar{\mu}_g \bar{c}_t r_w^2}\right) - 3.23 + 0.869 s\right] \quad \text{..... (3.16)}$$

Using resbbl/day instead of STB/day, then we have

$$p_i - p_w = \frac{162.6 q_R \bar{\mu}_g}{kh}\left[\log\left(\frac{kt}{\phi \bar{\mu}_g \bar{c}_t r_w^2}\right) - 3.23 + 0.869 s\right] \quad \text{..... (3.17)}$$

Then we apply the superposition theorem for reservoir outflow equation during acid injection:

$$-\frac{2\pi kh}{\bar{\mu}_g}(p_i - p_w) = \sum_{j=1}^{n} \Delta q_R^j [p_D(t_D^n - t_D^{j-1})] + q_R^n s^n, \quad \text{..... (3.18)}$$

where

$$\Delta q_R^j = q_R^j - q_R^{j-1}, \quad \text{..... (3.19)}$$

$$t_D = \frac{4.395 \times 10^{-6} kt}{\phi \bar{\mu}_g \bar{c}_t r_w^2}, \quad \text{..... (3.20)}$$

and

$$p_D \approx \frac{1}{2}(\ln t_D + 0.80907). \quad \text{..... (3.21)}$$

Now t is in minutes. If the wellbore is divided into small segments of thickness h, then Eq. 3.18 can be applied for each segment as the acid injection imitates and early radial

flow pattern. The term q_{sR} (= q_R/h) is specific reservoir outflow defined in unit bpm/ft. After dividing Eq. 3.18 by h and rearranging, we get

$$-\frac{2\pi k}{\overline{\mu}_g}(p_i - p_w) = \sum_{j=1}^{n-1} \Delta q_{sR}^j [p_D(t_D^n - t_D^{j-1})] + \Delta q_{sR}^n p_D(t_D^n - t_D^{n-1}) + q_{sR}^n s^n \quad \text{..... (3.22)}$$

The above equation can further be rearranged by using Eq. 3.19 as

$$-\frac{2\pi k}{\overline{\mu}_g}(p_i - p_w) = \sum_{j=1}^{n-1} \Delta q_{sR}^j [p_D(t_D^n - t_D^{j-1})] + q_{sR}^{n-1} p_D(t_D^n - t_D^{n-1})$$

$$+ q_{sR}^n [p_D(t_D^n - t_D^{n-1}) + s^n] \quad \text{..... (3.23)}$$

Then solving for q_{sR}^n, we obtain

$$q_{sR}^n = -a_J(p_i - p_w) - b_J \quad \text{..... (3.24)}$$

where the coefficient, a_J an b_J are defined by Eqs. 3.25 and 3.26 respectively,

$$a_J = \frac{4.91816 \times 10^{-6} k}{\overline{\mu}_g [p_D(t_D^n - t_D^{n-1}) + s^n]} \quad \text{..... (3.25)}$$

and

$$b_J = \frac{\left[\sum_{j=1}^{n-1} \Delta q_{sR}^j p_D(t_D^n - t_D^{j-1})\right] - q_R^{n-1} p_D(t_D^n - t_D^{n-1})}{\overline{\mu}_g [p_D(t_D^n - t_D^{n-1}) + s^n]} \quad \text{..... (3.26)}$$

3.4 Fluid Interface Tracking Model

A model to track the interfaces created between various fluids was presented by Jones and Davies (1996) and Eckerfield et al. (2000). This acid placement model will use a discretized solution approach which is integrated with the reservoir out flow,

wormholing, and apparent skin factor models. **Fig. 3.2** depicts a part of the wellbore where the interface created between different fluids. Assuming piston-like displacement, the velocity of an interface located at z_{int} is given by

$$\frac{dz_{\text{int}}}{dt} = \left.\frac{q_w}{A'}\right|_{z=z_{\text{int}}}, \quad \text{..... (3.27)}$$

In discrete form the location of interface at time $(t + \Delta t)$ can be written as

$$z_{\text{int}}\big|_{t=t+\Delta t} = z_{\text{int}}\big|_{t=t} + \left.\frac{q_w}{A'}\right|_{z=z_{\text{int}}} \Delta t, \quad \text{..... (3.28)}$$

where

$$A' = \frac{A}{\cos\theta}, \quad \text{..... (3.29)}$$

A is the cross-sectional area of flow in the pipe, and θ is slant angle. Eq. 3.28 is solved by discretizing the wellbore into small segments and assuming constant q_{w} over each segment.

A gas well is filled with gas or kill/completion fluid as an initial condition. If a wellbore is filled with gas, an interface will move up from the bottom. If wellbore is filled with kill/completion fluid, an interface will move down from the top.

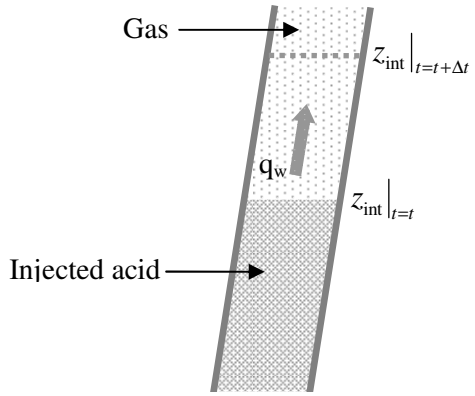

Fig. 3.2—Interface movement in the wellbore.

Once the interfaces and reservoir outflows in the wellbore parts are estimated, it is necessary to get the growth of wormhole during the injection time. A wormholing model is applied with injection volume or rate as input to get the wormhole growth. Penetration of wormhole is calculated by integrating growth in every small time step.

3.5 Wormholing Model

Models for predicting wormhole propagation have been widely discussed in the literature. Tardy et al. (2007) categorize the models in the following way:

I. 1D-averaged models

II. Discrete models

III. Darcy-scale 2D and 3D continuum models

IV. Multi-pore scale network models

Most models are usually successful in predicting wormhole growth under idealized conditions in the laboratory: linear core flow tests, one main wormhole, simple fluids

like HCl with known rheology and reactivity, etc. In the design of an acid treatment, however, these models are less useful because they cannot handle the complex field conditions such as: redial flow, multiple wormholes, complex fluids such as emulsified acids or foams, etc.

In this study, the semi-empirical model by Buijse and Glasbergen (2005) is used. This model can be applied to acidizing not only in oil wells but also in gas wells because the dependence on parameters such as rock properties, temperature, acid type and concentration is incorporated by fitting the model to the result of a laboratory experiment.

In the model, the growth rate of the wormhole front, V_{wh}, is expressed as a function of the interstitial fluid velocity, V_i:

$$V_{wh} = W_{eff} \cdot V_i^{2/3} \cdot B(V_i) \quad \text{..... (3.30)}$$

The constant W_{eff} in Eq. 3.30 is the wormhole efficiency factor which can be determined experimentally. The B-function in Eq. 3.30 describes the compact dissolution regime at low values of V_i. A convenient expression for B (V_i) is found to be:

$$B(V_i) = [1 - \exp(-W_B \cdot V_i^2)]^2 \quad \text{..... (3.31)}$$

At high values of V_i, the B-function is equal to 1, and has no effect on V_{wh}. When V_i is less than the optimum interstitial velocity, $V_{i\text{-}opt}$, the B-function has a value < 1, and has an inhibiting effect on the wormhole growth rate. The constant W_B is the wormhole B-factor. Its value is directly related to the optimum injection rate. An expression for the pore volumes to break through, PV_{bt}, is given by

$$PV_{bt} = \frac{V_i}{V_{wh}} \quad \text{..... (3.32)}$$

Substituting Eq. 3.30 into Eq. 3.32, we obtain

$$PV_{\mathrm{bt}} = \frac{V_{\mathrm{i}}^{1/3}}{W_{\mathrm{eff}} \cdot B(V_{\mathrm{i}})} \quad \text{..... (3.33)}$$

The constants, W_{eff} and W_{B}, can be determined experimentally by fitting Eq. 3.30 or 3.33 to the result of linear coreflood tests. For example, **Fig. 3.3** displays the results of such a fit. This procedure must be done numerically. Although the accuracy is less compared to a direct fit of a curve, the following equations give acceptable values:

$$W_{\mathrm{eff}} = \frac{V_{\mathrm{i-opt}}^{1/3}}{PV_{\mathrm{bt-opt}}} \quad \text{..... (3.34)}$$

and

$$W_{\mathrm{B}} = \frac{4}{V_{\mathrm{i-opt}}^{2}} \quad \text{..... (3.35)}$$

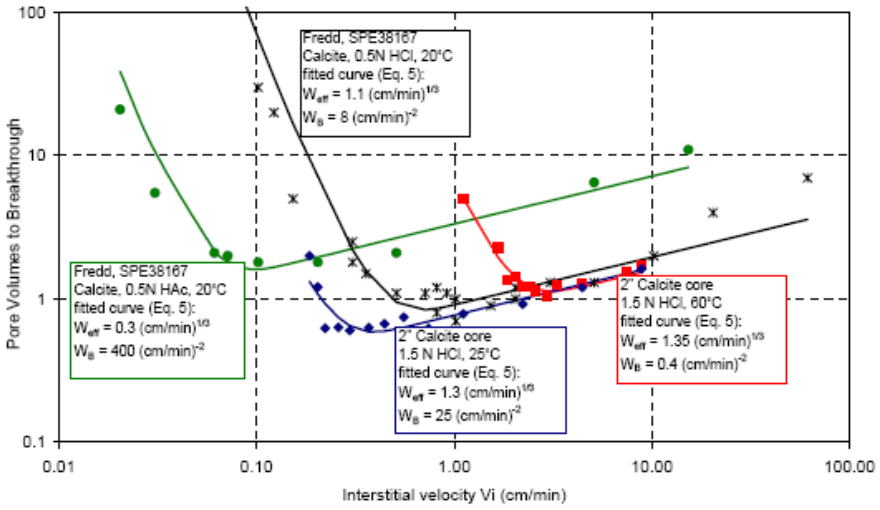

Fig. 3.3—Coreflood test results and numerical data fit (from Buijse and Glasbergen, 2005).

In radial geometry, V_i is given by

$$V_i(r) = \frac{q_R}{2\pi r h \phi} \quad \text{..... (3.36)}$$

Hence interstitial velocity changes with respect to radial distance. In addition, skin reduction affects flow rates. Therefore, it is needed to calculate the growth rate of wormhole front by Eq. 3.30 at each time step.

3.6 Apparent Skin Factor Model

3.6.1 Introduction

When acidizing a gas well, injection of liquid phase (acid) strongly affects the apparent skin factor depends on the viscosity difference between the reservoir fluid (gas) and injected fluid (acid). On the basis of this, Zhu et al. presented the following apparent skin factor model:

$$s_{app} = s_d + s_{vis,} \quad \text{..... (3.37)}$$

where

$$s_{vis} = \left(\frac{\mu_{acid}}{\mu_g} - 1 \right) \ln \frac{r_{acid}}{r_w} \quad \text{..... (3.38)}$$

In Eq. 3.38, μ_{acid} is acid viscosity in cp, μ_g is gas viscosity in cp, and r_{acid} is radius penetrated by acid in ft. This might work for sandstone formations, but not for carbonate formations since the pressure drop through a wormholed region is overestimated in Eq. 3.38. Because the wormholes created in carbonates are such big channels, it is generally assumed that the pressure drop through the wormholed region is negligible. Hence it is

not needed to evaluate the viscous skin effect in the wormholed region. As discussed in section 2, relative permeability difference should be accounted for as well. In the next section, a new apparent skin factor model is presented.

3.6.2 Derivation of Apparent Skin Factor Model

As discussed in Section 3.3, we assume a piston-like displacement. Hence gas saturation in the acid invaded zone is critical gas saturation, which means that gas is immobile. We derive an apparent skin factor model by following Hawkins' way (1956) in which steady-state flow is assumed in the vicinity of the wellbore. According to Brownscombe and Collins (1950), this assumption is valid because almost no difference between compressible and incompressible steady-state flow in the vicinity of the wellbore and the small volume of fluid in the vicinity of the wellbore makes unsteady-state mechanics unnecessary.

We have five different cases. We derive the equation for each case.

(i) $r_{wh} \le r_{spent} \le r_d$

In this case, both spent acid front and wormhole front terminate within the damage region and spent acid front is ahead of wormhole front (**Fig. 3.4 (a)**). Then a steady-state pressure drop between the outer boundary pressure (p_d) and the well would result in a $p_{wf,ideal}$ given by

$$p_d - p_{wf,ideal} = \frac{q\mu_g}{2\pi k k^{\circ}_{rg}} \ln \frac{r_d}{r_w}, \quad \text{..... (3.39)}$$

where k is original permeability in md, k_{rg}° is endpoint relative permeability to gas, and r_d is radius of damage zone. Though, the real bottomhole pressure is related by

$$p_d - p_{wf,real} = \frac{q\mu_{acid}}{2\pi k_\infty k_{ra}^{\circ} h}\ln\frac{r_{wh}}{r_w} + \frac{q\mu_{acid}}{2\pi k_d k_{ra}^{\circ} h}\ln\frac{r_{spent}}{r_{wh}} + \frac{q\mu_g}{2\pi k_d k_{rg}^{\circ}}\ln\frac{r_d}{r_{spent}}, \quad \text{..... (3.40)}$$

where r_{spent} is radius at spent acid front in ft, and k_{ra}° is endpoint relative permeability to acid. The difference between $p_{wf,ideal}$ and $p_{wf,real}$ is exactly the pressure drop due to the ski effect, Δp_s. Therefore, from Eqs. 3.39 and 3.40,

$$\begin{aligned}\Delta p_s &= \frac{q\mu_g}{2\pi k k_{rg}^{\circ}} s_{app} \\ &= \frac{q\mu_{acid}}{2\pi k_\infty k_{ra}^{\circ} h}\ln\frac{r_{wh}}{r_w} + \frac{q\mu_{acid}}{2\pi k_d k_{ra}^{\circ} h}\ln\frac{r_{spent}}{r_{wh}} + \frac{q\mu_g}{2\pi k_d k_{rg}^{\circ}}\ln\frac{r_d}{r_{spent}} - \frac{q\mu_g}{2\pi k k_{rg}^{\circ}}\ln\frac{r_d}{r_w}.\end{aligned}$$

..... (3.41)

Assuming k_∞ is infinite and solving for s_{app}, we finally obtain

$$s_{app} = \frac{k k_{rg}^{\circ}\mu_{acid}}{k_d k_{ra}^{\circ}\mu_g}\ln\frac{r_{spent}}{r_{wh}} + \frac{k}{k_d}\ln\frac{r_d}{r_{spent}} - \ln\frac{r_d}{r_w}. \quad \text{..... (3.42)}$$

In Eq. 3.42, the first term accounts for both damage effect and mobility difference effect while the second term accounts for only damage effect.

(ii) $r_{wh} \le r_d \le r_{spent}$

In this case, spent acid front terminates outside the damage zone while wormhole front terminates within the damage zone (**Fig. 3.4 (b)**). The ideal pressure drop is given by

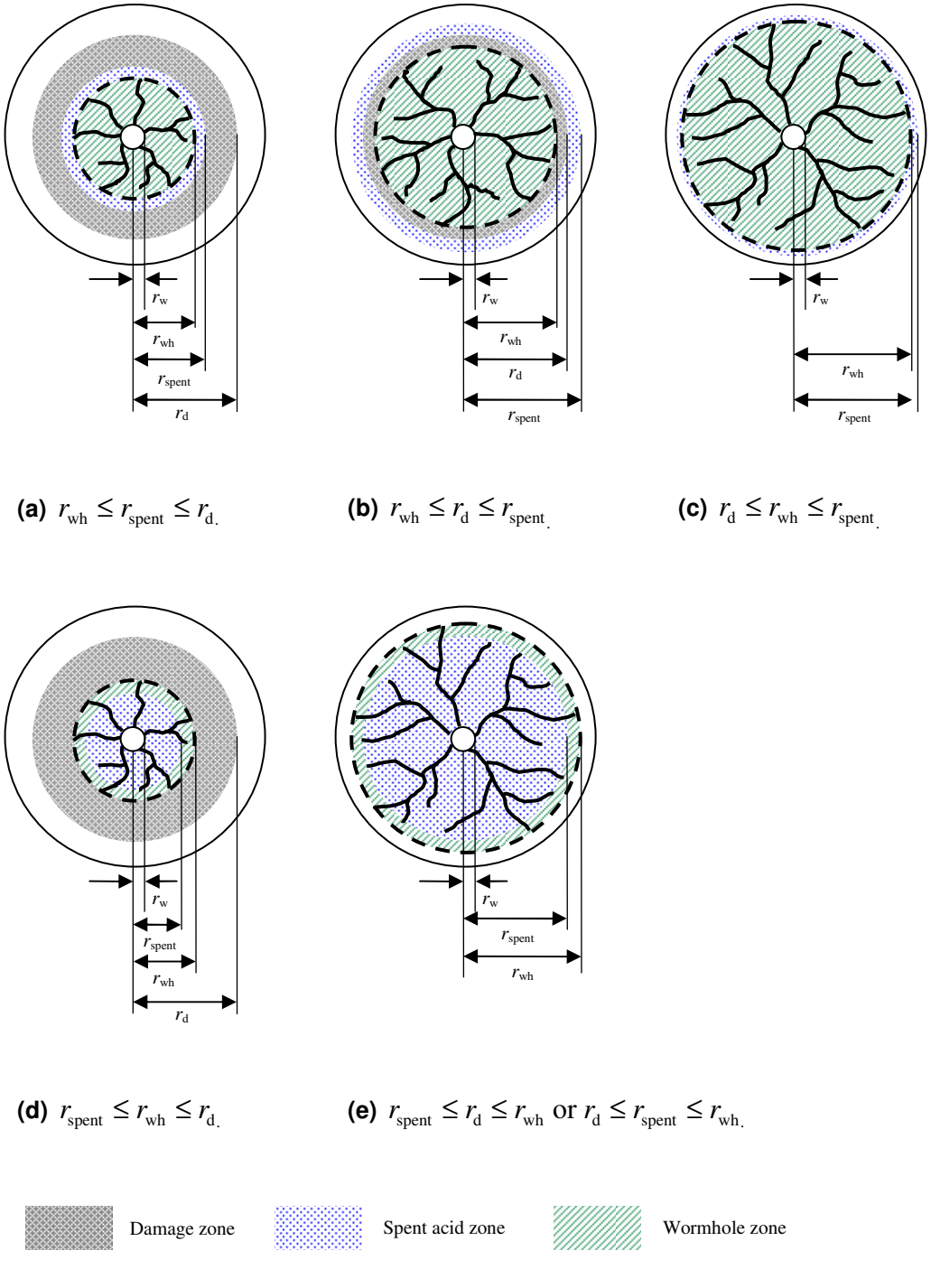

Fig. 3.4—Schematics of near-wellbore zone while acidizing in a gas well.

$$p_{\text{spent}} - p_{\text{wf,ideal}} = \frac{q\mu_{\text{g}}}{2\pi k k^{\circ}_{\text{rg}}} \ln \frac{r_{\text{spent}}}{r_{\text{w}}} \quad (3.43)$$

The real bottomhole pressure is related by

$$p_{\text{spent}} - p_{\text{wf,real}} = \frac{q\mu_{\text{acid}}}{2\pi k_{\infty} k^{\circ}_{\text{ra}} h} \ln \frac{r_{\text{wh}}}{r_{\text{w}}} + \frac{q\mu_{\text{acid}}}{2\pi k_{d} k^{\circ}_{\text{ra}} h} \ln \frac{r_{\text{d}}}{r_{\text{wh}}} + \frac{q\mu_{\text{acid}}}{2\pi k k^{\circ}_{\text{ra}}} \ln \frac{r_{\text{spent}}}{r_{\text{d}}} \quad \text{..... (3.44)}$$

Using Eqs. 3.43 and 3.44, s_{app} is given by

$$s_{\text{app}} = \frac{k k^{\circ}_{\text{rg}} \mu_{\text{acid}}}{k_{d} k^{\circ}_{\text{ra}} \mu_{\text{g}}} \ln \frac{r_{\text{d}}}{r_{\text{wh}}} + \frac{k^{\circ}_{\text{rg}}}{k^{\circ}_{\text{ra}}} \ln \frac{r_{\text{spent}}}{r_{\text{d}}} - \ln \frac{r_{\text{spent}}}{r_{\text{w}}} \quad \text{..... (3.45)}$$

(iii) $r_{\text{d}} \le r_{\text{wh}} \le r_{\text{spent}}$

In this case, both spent acid front and wormhole front terminate outside the damage region (**Fig. 3.4 (c)**). The ideal pressure drop is given by Eq. 3.43. The real bottomhole pressure is related by

$$p_{\text{spent}} - p_{\text{wf,real}} = \frac{q\mu_{\text{acid}}}{2\pi k_{\infty} k^{\circ}_{\text{ra}} h} \ln \frac{r_{\text{wh}}}{r_{\text{w}}} + \frac{q\mu_{\text{acid}}}{2\pi k k^{\circ}_{\text{ra}}} \ln \frac{r_{\text{spent}}}{r_{\text{wh}}} \quad \text{..... (3.46)}$$

Using Eqs. 3.43 and 3.46, s_{app} is given by

$$s_{\text{app}} = \frac{k^{\circ}_{\text{rg}} \mu_{\text{acid}}}{k^{\circ}_{\text{ra}} \mu_{\text{g}}} \ln \frac{r_{\text{spent}}}{r_{\text{wh}}} - \ln \frac{r_{\text{spent}}}{r_{\text{w}}} \quad \text{..... (3.47)}$$

According to Eq. 3.46, even if wormhole front breaks through, there is still mobility difference effect. The pressure drop due to mobility difference is equivalent to the first term in Eq. 2.1.

(iv) $r_{\text{spent}} \le r_{\text{wh}} \le r_{\text{d}}$

In this case, both spent acid front and wormhole front terminate within the damage region and wormhole front is ahead of spent acid front (**Fig. 3.4 (d)**). The ideal pressure drop is given by Eq. 3.39. The real bottomhole pressure is related by

$$p_{\mathrm{d}} - p_{\mathrm{wf,real}} = \frac{q\mu_{\mathrm{acid}}}{2\pi k_{\infty} k_{\mathrm{ra}}^{\circ} h} \ln \frac{r_{\mathrm{wh}}}{r_{\mathrm{w}}} + \frac{q\mu_{\mathrm{g}}}{2\pi k_{\mathrm{d}} k_{\mathrm{rg}}^{\circ}} \ln \frac{r_{\mathrm{d}}}{r_{\mathrm{wh}}} \quad \text{..... (3.48)}$$

Using Eqs. 3.39 and 3.48, s_{app} is given by

$$s_{\mathrm{app}} = \frac{k}{k_{\mathrm{d}}} \ln \frac{r_{\mathrm{d}}}{r_{\mathrm{wh}}} - \ln \frac{r_{\mathrm{d}}}{r_{\mathrm{w}}} \quad \text{..... (3.49)}$$

In this case there is no effect of mobility difference.

(v) $r_{\mathrm{spent}} \le r_{\mathrm{d}} \le r_{\mathrm{wh}}$ or $r_{\mathrm{d}} \le r_{\mathrm{spent}} \le r_{\mathrm{wh}}$

In this case, wormhole front terminate outside the damage region and wormhole front is ahead of spent acid front (**Fig. 3.4 (e)**). The ideal pressure drop is given by

$$p_{\mathrm{wh}} - p_{\mathrm{wf,ideal}} = \frac{q\mu_{\mathrm{g}}}{2\pi k k_{\mathrm{rg}}^{\circ}} \ln \frac{r_{\mathrm{wh}}}{r_{\mathrm{w}}} \quad \text{..... (3.50)}$$

The real bottomhole pressure is related by

$$p_{\mathrm{wh}} - p_{\mathrm{wf,real}} = \frac{q\mu_{\mathrm{acid}}}{2\pi k_{\infty} k_{\mathrm{ra}}^{\circ} h} \ln \frac{r_{\mathrm{wh}}}{r_{\mathrm{w}}} \quad \text{..... (3.51)}$$

Using Eqs. 3.50 and 3.51, s_{app} is given by

$$s_{\mathrm{app}} = -\ln \frac{r_{\mathrm{wh}}}{r_{\mathrm{w}}} \quad \text{..... (3.52)}$$

3.7 Slant Skin Effect

Deviated holes are drilled to increase the surface area exposed to formation, thereby improving the well productivity. Several researchers have developed correlations to determine the slant skin factor, s_θ. Cinco-Ley et al. (1975) defined this version of the skin factor as functions of slant angle, horizontal permeability and vertical permeability:

$$s_\theta = -\left(\frac{\theta'_w}{41}\right)^{2.06} - \left(\frac{\theta'_w}{56}\right)^{1.865} \times \log\left(\frac{h}{100 \cdot r_w}\sqrt{\frac{k_H}{k_V}}\right) \quad \text{..... (3.53)}$$

for $0^\circ \le \theta'_w \le 75^\circ$, where

$$\theta'_w = \tan^{-1}\left(\sqrt{\frac{k_V}{k_H}}\tan\theta_w\right) \quad \text{..... (3.54)}$$

Besson (1990) studied performance of slanted and horizontal wells using the definition of a geometrical skin. Besson obtained the following correlation of skin for slanted wells:

$$s_\theta = \ln\left(\frac{4r_w\cos\theta}{h\gamma}\sqrt{\frac{k_V}{k_H}}\right) + \frac{\cos\theta}{\gamma}\ln\left(\frac{h}{2r_w(1+1/\gamma)}\sqrt{\frac{k_H\gamma}{k_V\cos\theta}}\right) \quad \text{..... (3.55)}$$

where

$$\gamma = \sqrt{\cos^2\theta + \frac{k_V}{k_H}\sin^2\theta} \quad \text{..... (3.56)}$$

Rogers and Economides presented a correlation for skin factor to account for slant deviation:

$$s_\theta = -1.64 \frac{(\sin\theta)^{1.77} (h/r_w)^{0.184}}{(\sqrt{k_H/k_V})^{0.821}}, \quad \text{for } \sqrt{\frac{k_H}{k_V}} < 1, \quad \text{..... (3.57)}$$

and

$$s_\theta = -2.48 \frac{(\sin\theta)^{5.87} (h/r_w)^{0.152}}{(\sqrt{k_H/k_V})^{0.964}}, \quad \text{for } \sqrt{\frac{k_H}{k_V}} \geq 1. \quad \text{..... (3.58)}$$

The three models are semi-analytical models. We compare these models using different indices of permeability anisotropy ($I_{\text{ani}} = \sqrt{k_H/k_V}$). **Figs. 3.5 (a)** through **(c)** show the results. Cinco-Ley et al. model and Besson model give almost same results while Rogers and Economides model's result differs from other results. In addition, since Cinco-Ley et al. model has a limitation of slant angle range, we use Besson model.

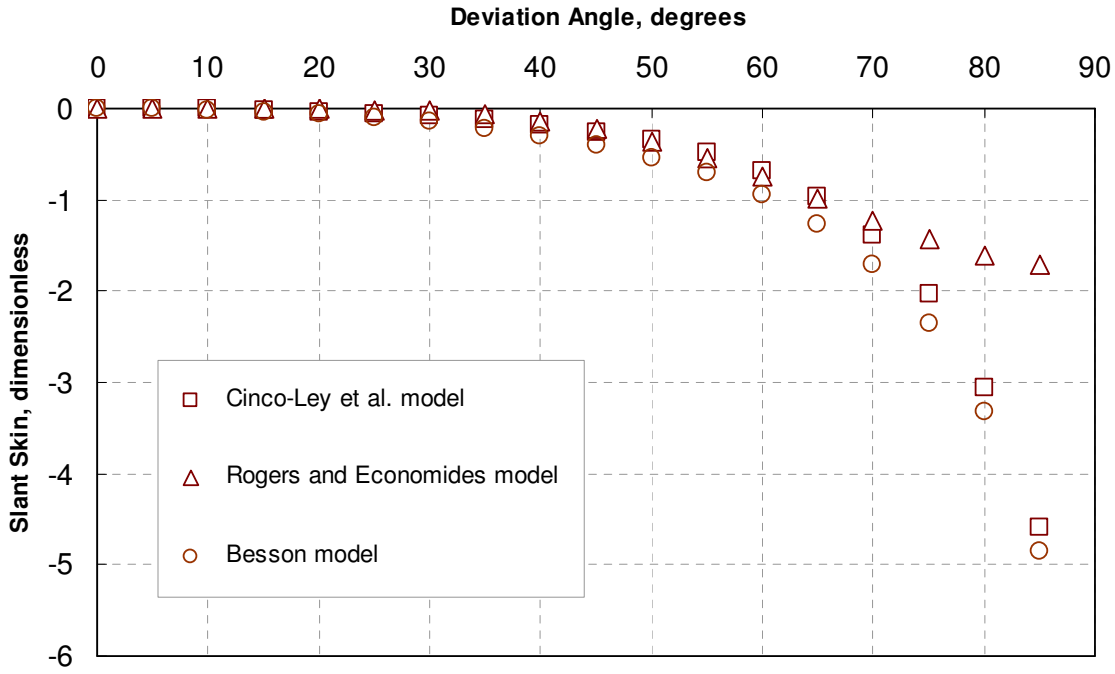

Fig. 3.5 (a)—Comparison of slant skin models (k_H = 10 md and k_V = 1 md).

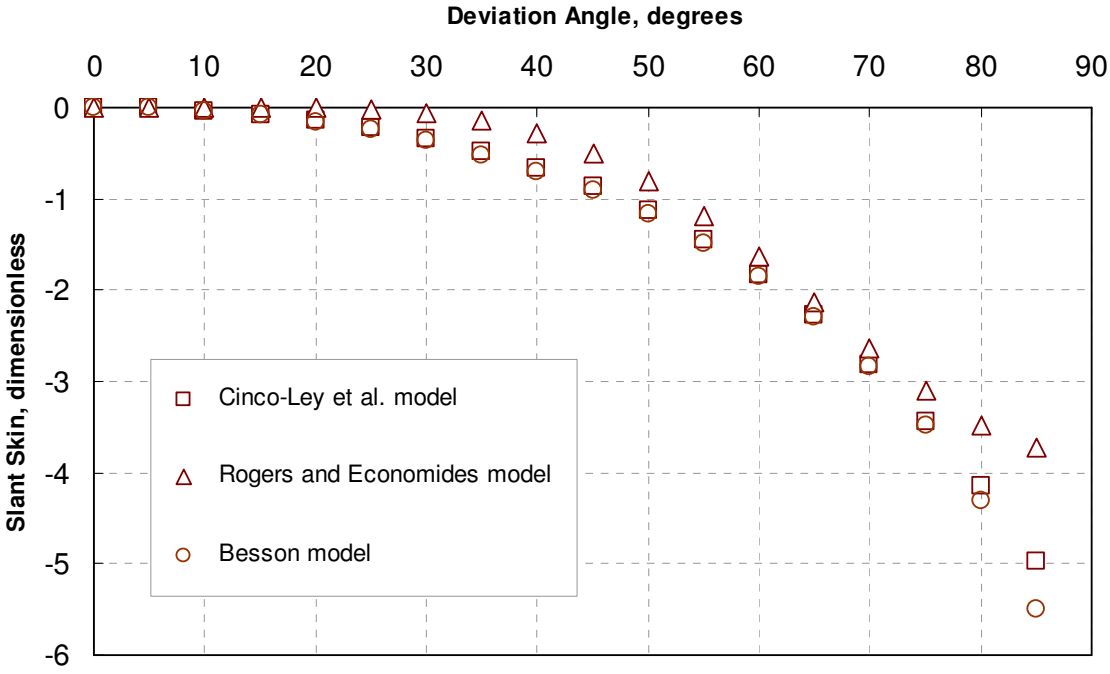

Fig. 3.5 (b)—Comparison of slant skin models (k_H = 10 md and k_V = 5 md).

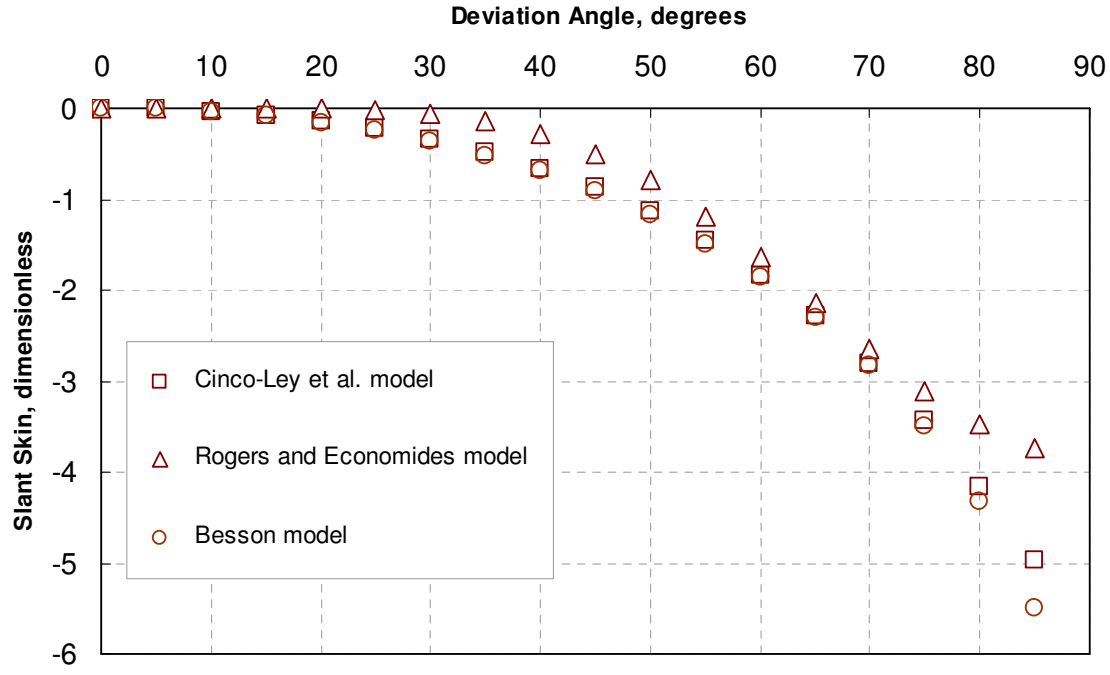

Fig. 3.5 (c)—Comparison of slant skin models (k_H = 10 md and k_V = 10 md).

3.8 Section Summary

In this section, we presented an acid placement model for gas wells which includes:

- Wellbore flow model.
- Reservoir outflow model.
- Fluid interface tracking model.
- Wormholing model.
- Apparent skin factor model.
- Slant skin factor model.

We show a method to solve the model equations in the next section.

4. ACID PLACEMENT SIMULATOR

4.1 Solution of Acid Placement Model

To solve the problem of matrix acid placement in a gas well, all models presented in the previous section are integrated and solved in a discretized manner in time and space (discussed in Sec. 4.2). Initial conditions to solve the system of equations are defined as:

$$q_w(z,0) = 0, \quad \text{..... (4.1)}$$

and

$$p_w(z,0) = p_i. \quad \text{..... (4.2)}$$

Eq. 4.1 explains that the initial wellbore flow rate at any points is zero. To satisfy this condition, the initial pressure is equal to the initial reservoir pressure. If the wellbore is filled with kill/completion fluid, then we set the following conditions along with the above initial conditions:

$$q_w(0,t) = q_{\text{inj}}(t), \quad \text{..... (4.3)}$$

and

$$q_w(z = z_{\text{bottom}}, t) = 0. \quad \text{..... (4.4)}$$

If the wellbore is filled with gas, then we set the following conditions along with the above initial conditions:

$$q_w(0,t) = 0, \quad \text{..... (4.5)}$$

and

$$q_w(z = z_{\text{bottom}}, t) = q_{\text{inj}}(t). \quad \text{..... (4.6)}$$

Although there is two-phase flow in this condition, we consider single-phase flow for each segment. We assume that the injected acid falls down to the bottom of the wellbore instantaneously and it works as a source for the acid-filled part of the wellbore. For convenience, we treat it not as a source term but a boundary condition (Eq. 4.6) since the real flow rate at the boundary is zero. We must use a big enough time step to make the assumption valid.

The followings are the steps to solve the model equations:

1. Divide the slanted wellbore into small segments.
2. Apply the initial and boundary conditions.
3. Use the apparent skin factor model and slant skin model to get the total skin factor for the reservoir at each segment.
4. Solve the pressure drop equation and the reservoir out flow equation to get p_w, q_w, q_R.
5. Use the interface tracking model to get the interface locations.
6. Calculate the volume of acid injected into each segment during the time step from the flow distribution and interface tracking.
7. Use the wormhole model to get the penetration of wormhole in each segment.
8. Go back to step 3 and loop through the skin factor calculation using new wormhole length.

In the next section, we show the acid placement model in a discretized form and then provide the details about how to implement step 4.

4.2 Discretization

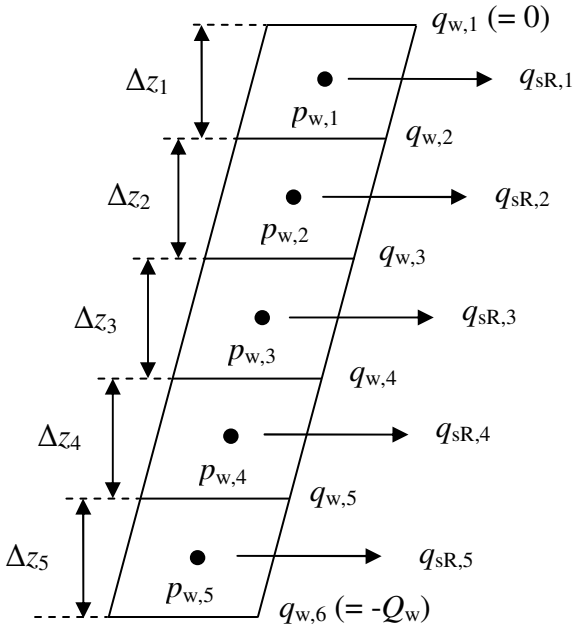

Fig. 4.1—A schematic of segmented wellbore.

Fig. 4.1 provides a schematic of segmented wellbore. In this example case the wellbore is divided into 5 segments. The wellbore pressure in each segment is defined as $p_{w,j}$, where j denotes the segment number. These segments can be of a uniform size or a non-uniform size. Height of each segment is defined as Δz_j and specific reservoir outflow from each segment is denoted as $q_{sR,i}$. The wellbore flow is defined as $q_{w,i}$ as it is defined at the faces of the grid blocks.

The wellbore pressure drop equation, Eq. 3.7, can be written in discretized form as

$$p_{w,j+1} - p_{w,j} = 0.433\gamma_a \frac{\Delta z_{j+1} + \Delta z_j}{2} \quad \text{for } j = 1, 2, 3, \text{ and, } 4. \quad \text{..... (4.7)}$$

Right hand side of Eq. 4.7 can be assumed constant. Hence, there is only one unknown, and $p_{w,j}$ is given by

$$p_{w,j} = p_{w,1} + 0.433\gamma_a \frac{\Delta z_1 + \Delta z_j + 2\sum_{k=2}^{j-1} \Delta z_k}{2} \equiv p_{w,1} + c_j, \quad \text{for j} = 2, 3, 4, \text{and, } 5. \quad \text{.. (4.8)}$$

In addition, we define $c_1 = 0$.

The equation which couples wellbore material balance and reservoir outflow, Eqs. 3.1 and 3.24 respectively, can be also written in discretized form as

$$q_{w,j+1} - q_{w,j} = \Delta z_j [a_{J,j}(p_{i,j} - p_{w,j}) + b_{J,j}] \quad \text{for j} = 1, 2, 3, 4, \text{and } 5. \quad \text{..... (4.9)}$$

Substituting Eq. 4.8 into Eq. 4.9, we obtain

$$q_{w,j+1} - q_{w,j} = \Delta z_j [a_{J,j}(p_{i,j} - p_{w,1} - c_j) + b_{J,j}] \quad \text{for j} = 1, 2, 3, 4, \text{and } 5. \quad \text{..... (4.10)}$$

After applying the boundary conditions for gas-filled wellbore (Eqs. 4.5 and 4.6), these equations can be set as

$$\begin{pmatrix} \Delta z_1 & 1 & 0 & 0 & 0 \\ \Delta z_2 & -1 & 1 & 0 & 0 \\ \Delta z_3 & 0 & -1 & 1 & 0 \\ \Delta z_4 & 0 & 0 & -1 & 1 \\ \Delta z_5 & 0 & 0 & 0 & -1 \end{pmatrix} \begin{pmatrix} p_{w,1} \\ q_{w,2} \\ q_{w,3} \\ q_{w,4} \\ q_{w,5} \end{pmatrix} = \begin{pmatrix} \Delta z_1 [a_{J,1}(p_{i,1} + c_1) + b_{J,1}] \\ \Delta z_2 [a_{J,2}(p_{i,2} + c_2) + b_{J,2}] \\ \Delta z_3 [a_{J,3}(p_{i,3} + c_3) + b_{J,3}] \\ \Delta z_4 [a_{J,4}(p_{i,4} + c_4) + b_{J,4}] \\ \Delta z_5 [a_{J,5}(p_{i,5} + c_5) + b_{J,5}] + Q_w \end{pmatrix} \quad \text{..... (4.11)}$$

This equation is linear. Hence it does not need iterative calculation.

4.3 Program Structure

The acid placement model has been developed in Fortran Programming language. **Fig. 4.2** shows the program structure. The wellbore is divided into various segments on the basis of input data, and large enough time step size to satisfy CFL condition is selected. Then, the solution matrix (Eq. 4.11) is constructed and solved at each time step. At a new time step, wormhole penetration and spent acid penetration are calculated, and a new total skin factor is calculated by using the skin models derived in section 3. Then, the solution matrix is constructed and solved, again.

The following equation is used to calculate radius at spent acid front in radial geometry:

$$r_{\text{spent}} = \sqrt{r_w^2 + \frac{V_{\text{acid}}}{\pi h \phi (1 - S_{gc})}}, \quad \text{..... (4.12)}$$

where V_{acid} is total volume of acid injected, and S_{gc} is critical gas saturation. In this equation, either porosity change or fluid loss is not accounted for. Hence, radius at spent acid front will be overestimated. Though, this might give us a good approximation because as discussed in section 2, the wormhole in the gas saturated core was observed to have less branching than that in the liquid saturated core.

The simulation ends when the time reaches to the end time. The output gives the pressure, wellbore flow rate, and injection rate at each segment for each time step. Those data are valuable information needed to evaluate the performance of acidizing process. A history match can then be performed for observed data and simulated data by varying the treatment schedule.

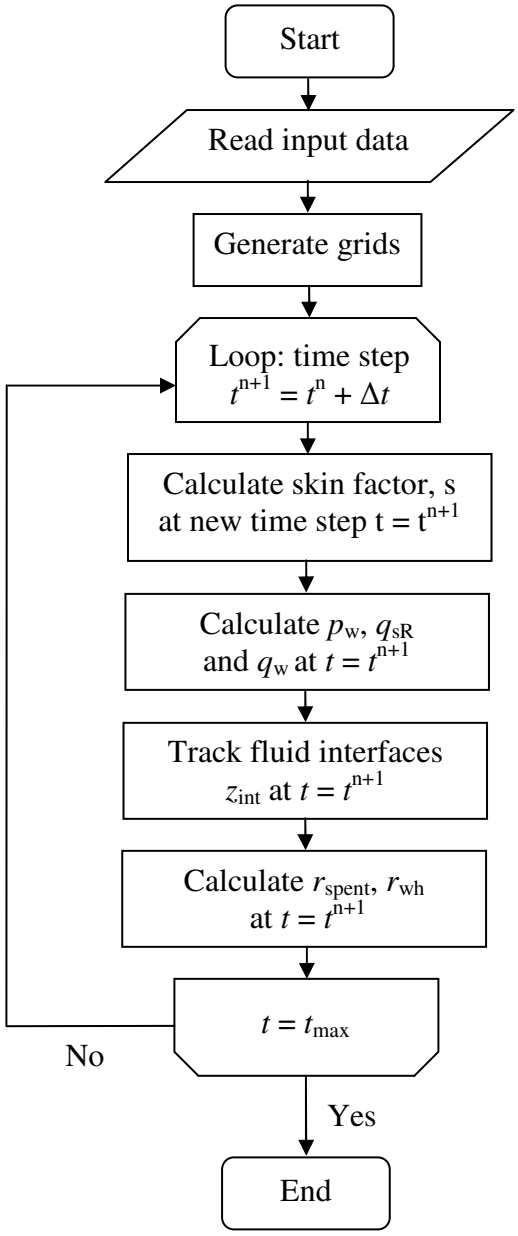

Fig. 4.2—Simulator flow chart.

5. HYPOTHETICAL EXAMPLES

5.1 One-Layer Case

5.1.1 Base Case

We implement sensitivity analysis. We see skin factor profile and flow rate profile with different reservoir thicknesses, original permeabilities, damage permeabilities, radii of damage region, optimal pore volumes to breakthrough, and optimal interstitial velocities. **Table 5.1** shows the base case data. In this analysis, wellbore pressure is set as a constant.

First, we show typical apparent skin factor profile and flow rate profile with the result from the base data. **Fig. 5.1** shows the skin factor profile. At the first discontinuous point spent acid front breaks through, and at the second discontinuous point wormhole front breaks through. We have an unusual value of skin factor because this skin factor accounts for not only damage skin effect but also mobility skin effect. We should notice that the skin factor is based on Eq.3.41. The flow rate profile (**Fig. 5.2**) also has two discontinuous points which are correspond to the discontinuous points in Fig. 5.2. The decrease of the flow rate is cause by the mobility difference skin effect.

In the next section, we see how each property affect the skin factor profile and flow rate profile.

Table 5.1—Base case data	
Wellbore data	
Well pressure, psi	5,600
Well radius, ft	0.328
Completion type	Openhole
Reservoir data	
Initial reservoir pressure, psi	5,315
Original permeability, md	100
Damage permeability, md	10
Radius of damage region, ft	1.5
Reservoir thickness, ft	50
Temperature, ^{o}F	220
Porosity, fraction	0.25
Gas viscosity at $p = p_i$, cp	0.0305
Gas compressibility at $p = p_i$, psi^{-1}	0.000107087
Endpoint gas relative permeability	0.9
Critical gas saturation, fraction	0.1
Optimal interstitial velocity, cm/min	0.3
Optimal pore volumes to breakthrough	1.0
Acid data	
Acid type	15% HCl
Acid viscosity, cp	0.445
Endpoint acid solution relative permeability	0.5

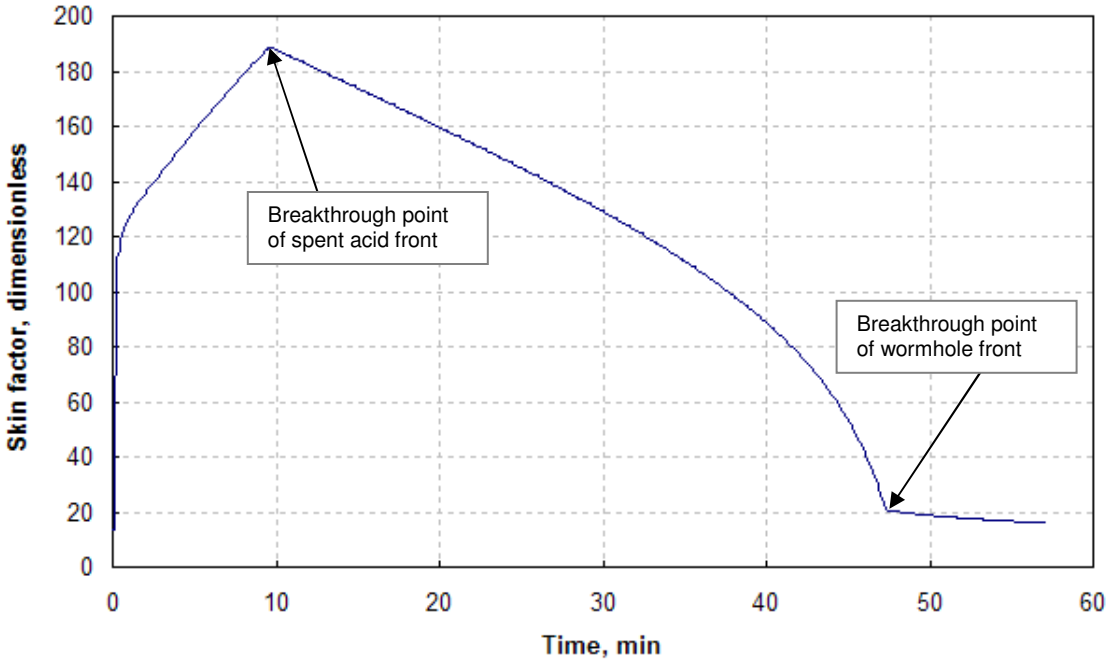

Fig. 5.1—Skin factor profile using base case data.

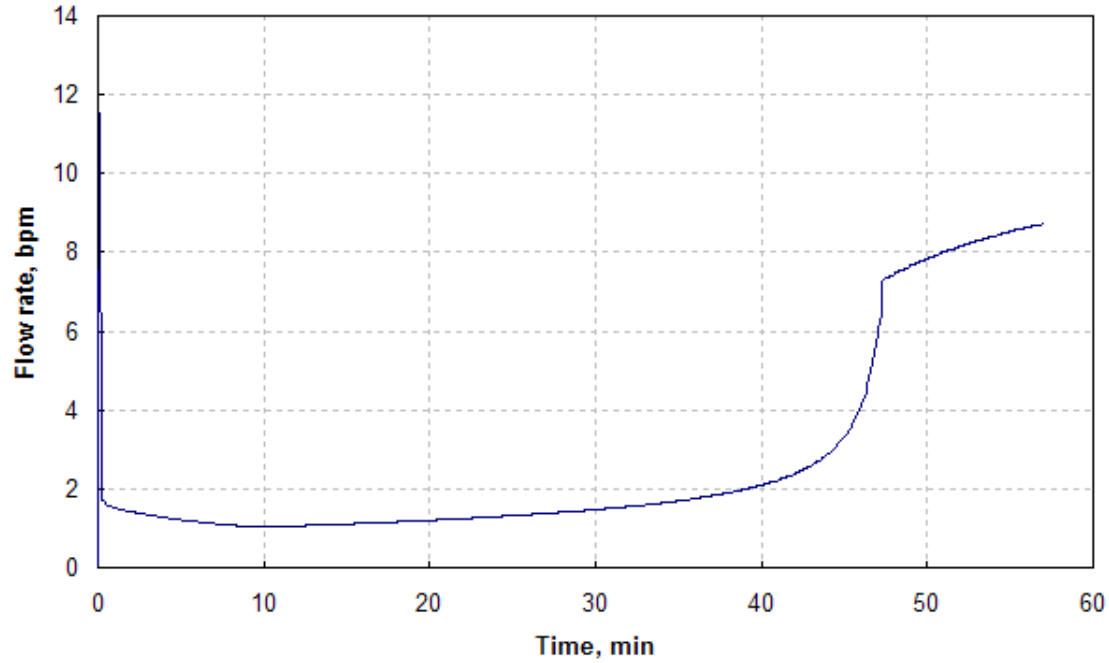

Fig. 5.2—Flow rate profile using base case data.

5.1.2 Sensitivity Analysis

(i) Reservoir thickness

Fig. 5.3 shows that reservoir thickness does not affect the apparent skin factor at all. Hence there is no effect on the flow rate profile (**Fig. 5.4**).

(ii) Original permeability

Apparent skin factor strongly depends on original permeability (**Fig. 5.5**) while flow rate does not (**Fig. 5.6**) before wormhole front breaks through. On the other hand, after wormhole front breaks through, apparent skin factor does not depend on original permeability while flow rate depends on original permeability. The results imply that pressure drop in acid invaded zone is bigger than that in gas zone and original permeability does not affect the flow rate much while wormhole terminates within the damage region.

(iii) Damage permeability

Fig. 5.7 shows that damage permeability affects apparent skin factor. Obviously damage permeability is one of the key factors of both wormhole front's and spent acid's front velocity. In our calculation, the bigger damage permeability we have, the larger amount of spent acid is ahead of wormhole and the more time is needed for wormhole to break through because of overestimation of r_{spent}. Flow rate also depends on damage permeability (**Fig. 5.8**).

(iv) Radius of damage region

In the same as damage permeability, radius of damage region strongly affects the apparent skin factor and flow rate (**Figs. 5.9** and **5.10**). The figures show that final apparent skin factor is almost constant. This may imply that the final value is dependent on the mobility difference between acid and gas.

Here, we must notice that a final apparent skin factor can be greater than the initial apparent skin factor. This does not mean there is still damage in the reservoir. There is mobility difference effect.

(v) Optimal pore volume to breakthrough

Optimal pore volume to breakthrough is one of input constants of wormholing model (Eq. 3.34). Hence this affects the wormhole growth. As **Fig. 5.11** shows, the smaller the optimal pore volume to breakthrough is, the smaller the difference of velocity between wormhole front and spent acid front is, i.e., the smaller volume of spent acid is ahead of wormhole. Hence, flow rate also depends on the optimal pore volume to breakthrough (**Fig. 5.12**).

(vi) Optimal interstitial velocity

Optimal interstitial velocity is also one of input constants of wormholing model (Eqs. 3.34 and 3.35). In the same as the optimal pore volumes to break through, it affects wormhole growth. According to **Fig. 5.13**, the bigger value the optimal interstitial value is, the smaller the apparent skin factor is and the bigger flow rate is (**Fig. 5.14**).

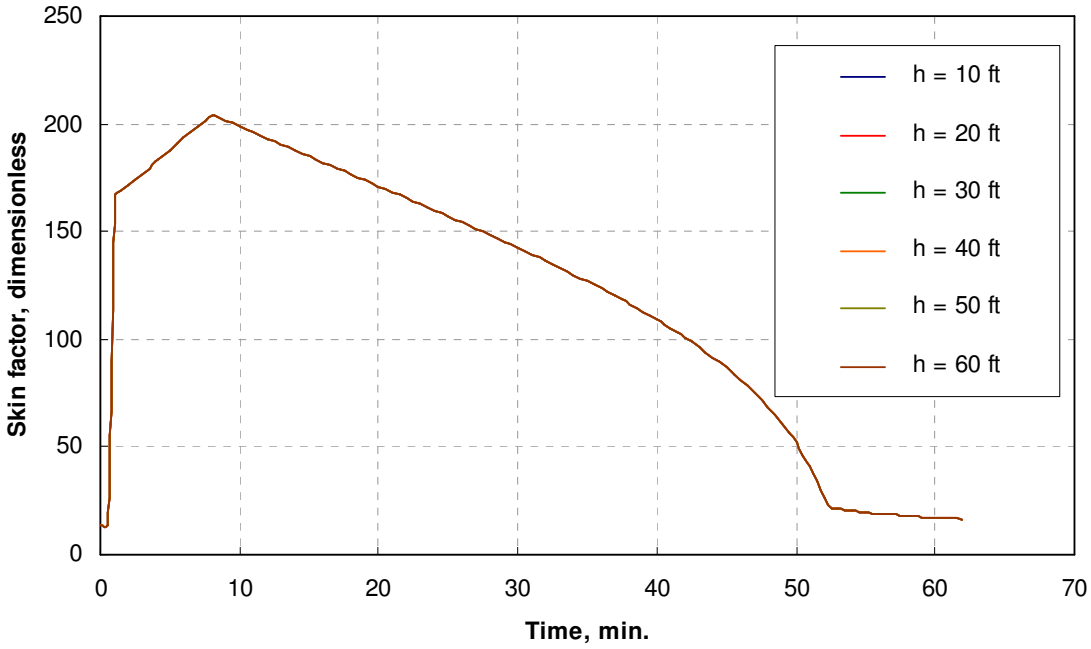

Fig. 5.3—A comparison of apparent skin factor profile among different reservoir thicknesses.

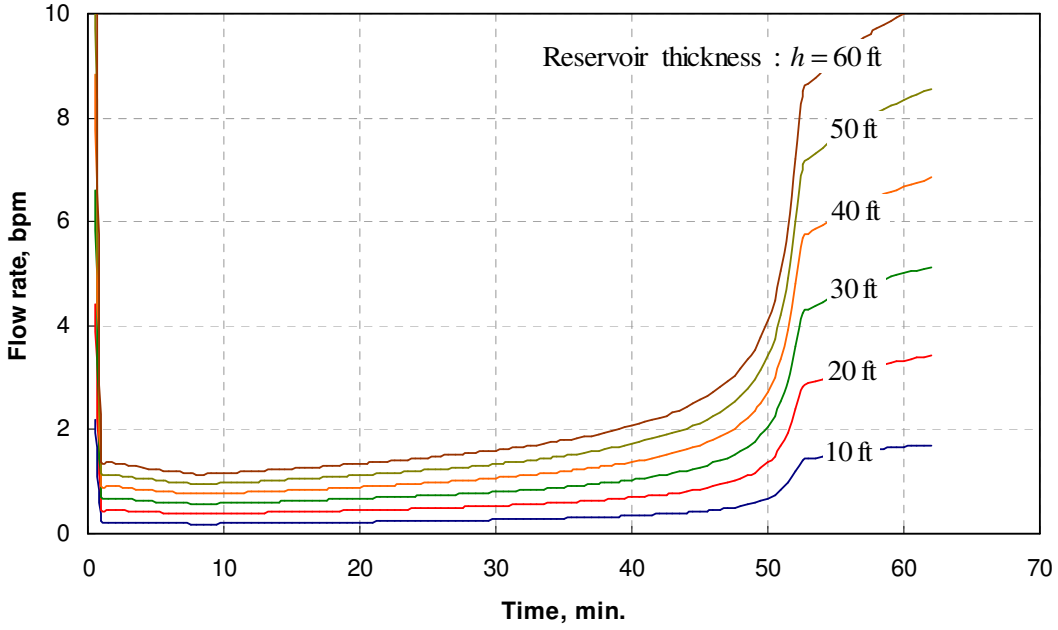

Fig. 5.4—A comparison of flow rate profile among different reservoir thicknesses.

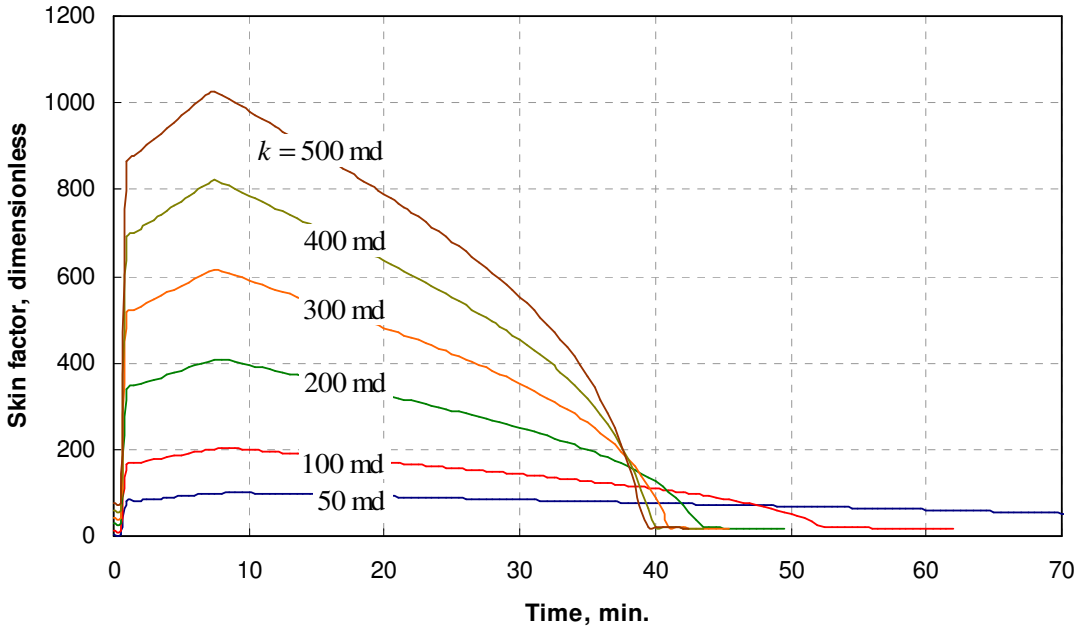

Fig. 5.5—A comparison of apparent skin factor profile among different original permeabilities.

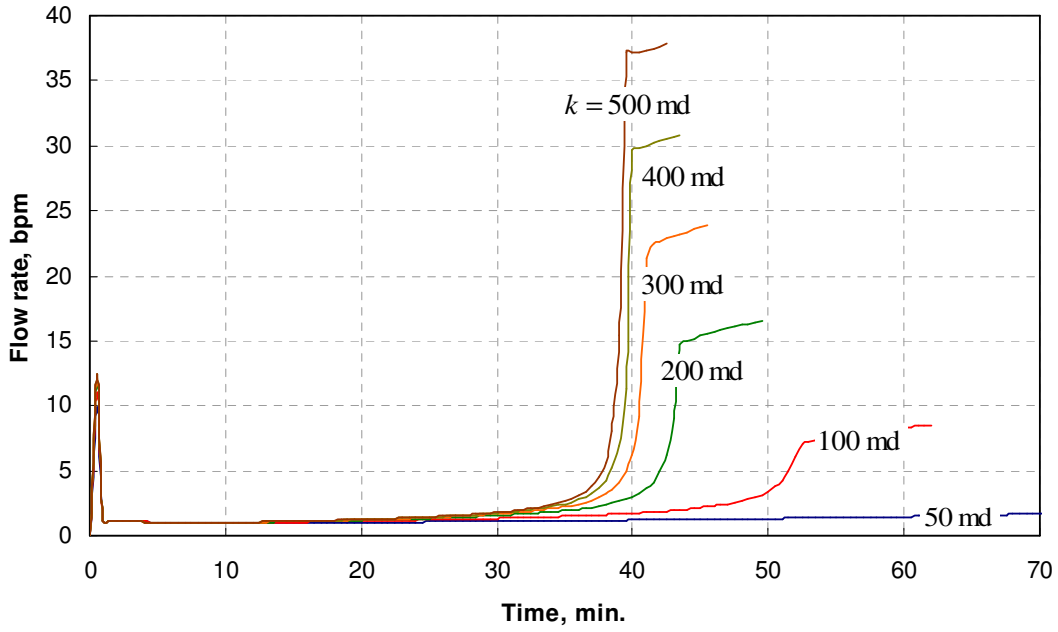

Fig. 5.6—A comparison of apparent flow rate profile among different original permeabilities.

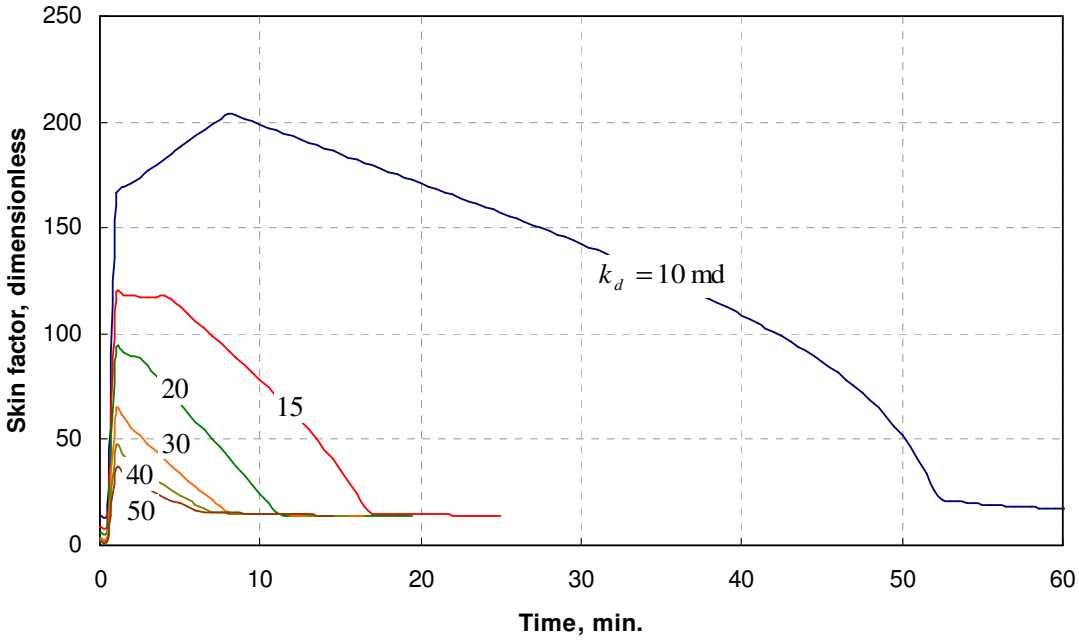

Fig. 5.7—A comparison of apparent skin factor profile among different damage permeabilities.

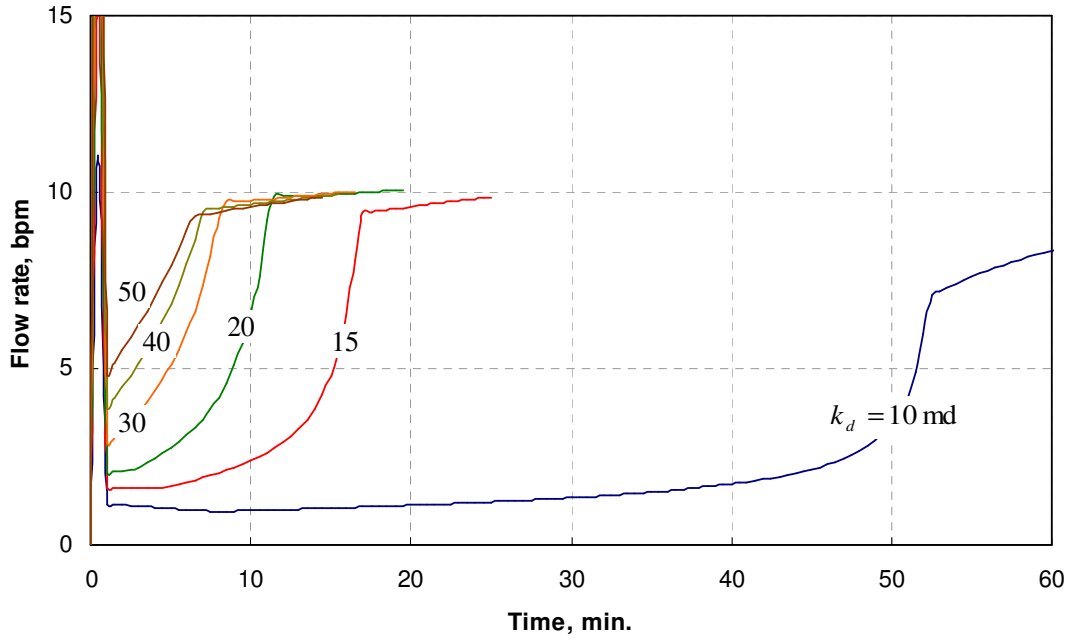

Fig. 5.8—A comparison of flow rate profile among different damage permeabilities.

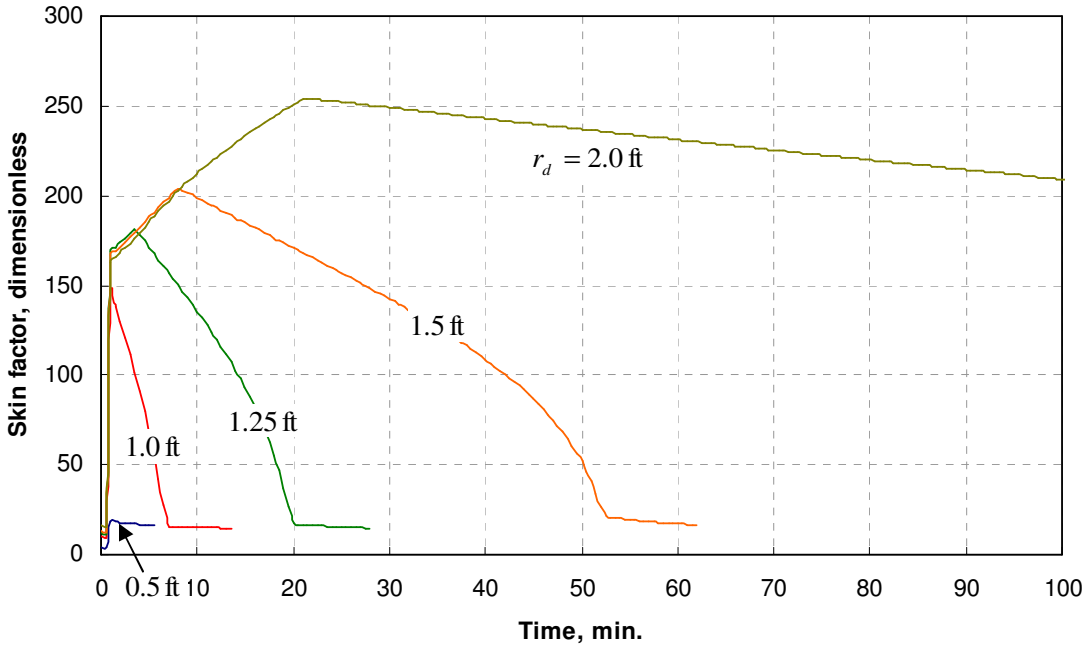

Fig. 5.9—A comparison of apparent skin factor profile among different radii of damage region.

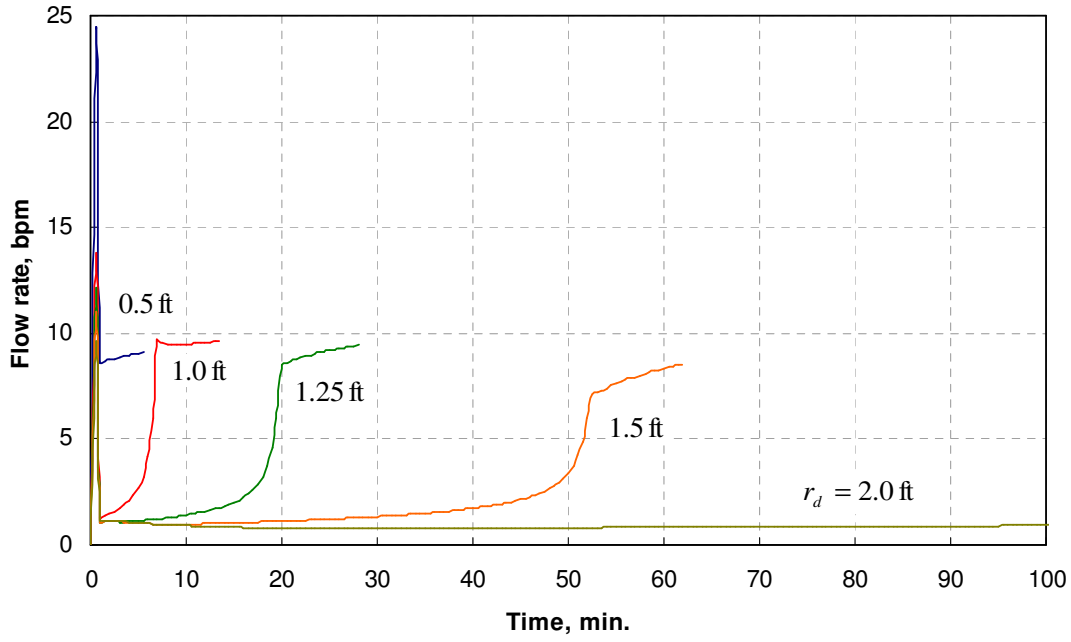

Fig. 5.10—A comparison of flow rate profile among different radii of damage region.

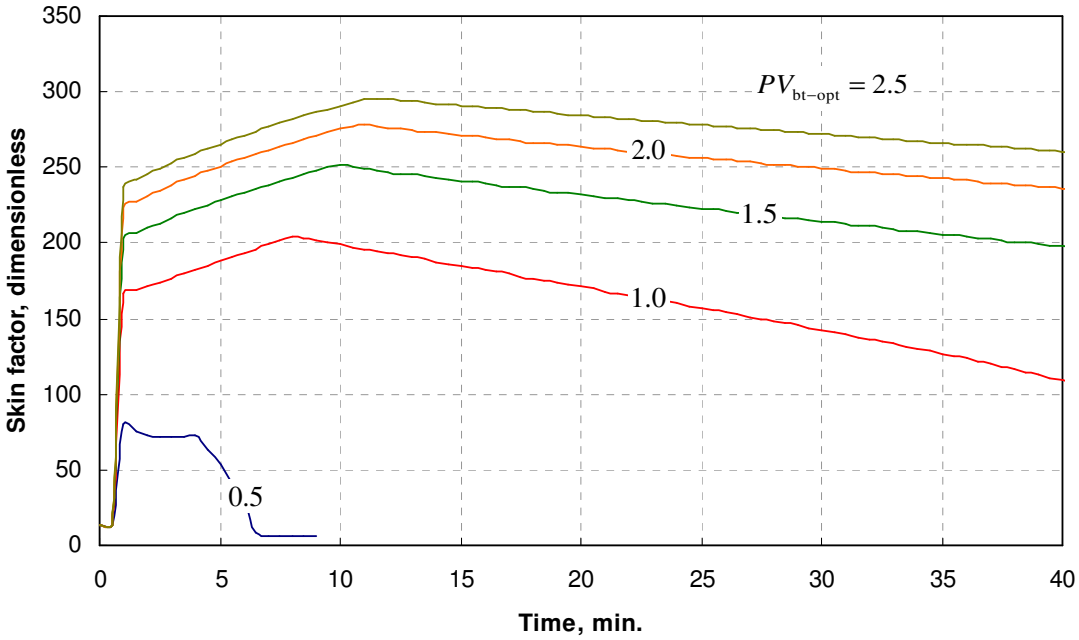

Fig. 5.11—A comparison of apparent skin factor profile among different optimal pore volumes to breakthrough.

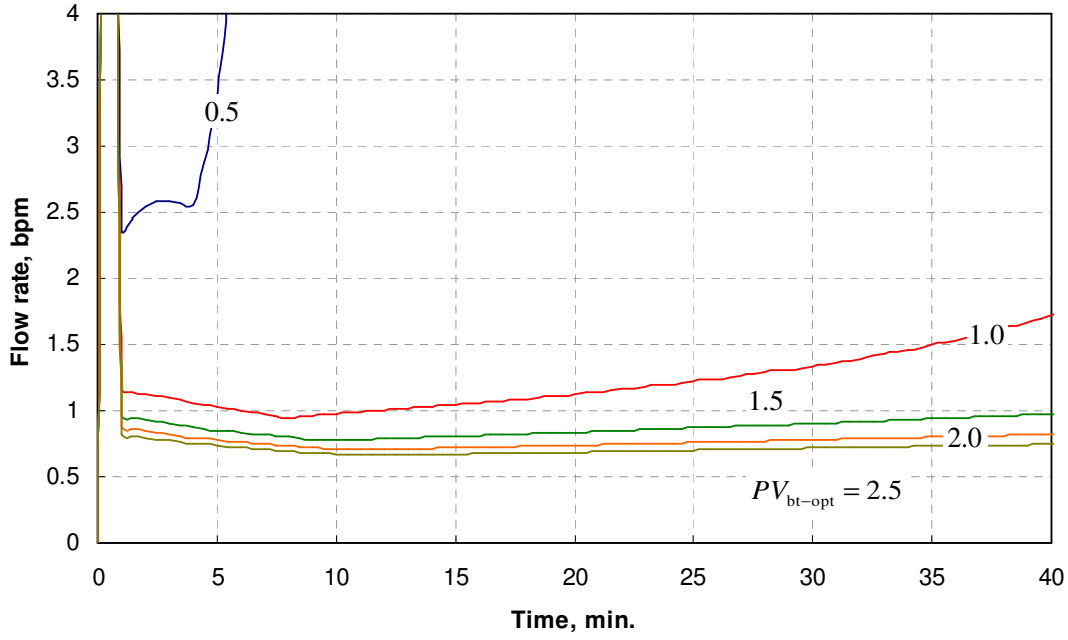

Fig. 5.12—A comparison of flow rate profile among different optimal pore volumes to breakthrough.

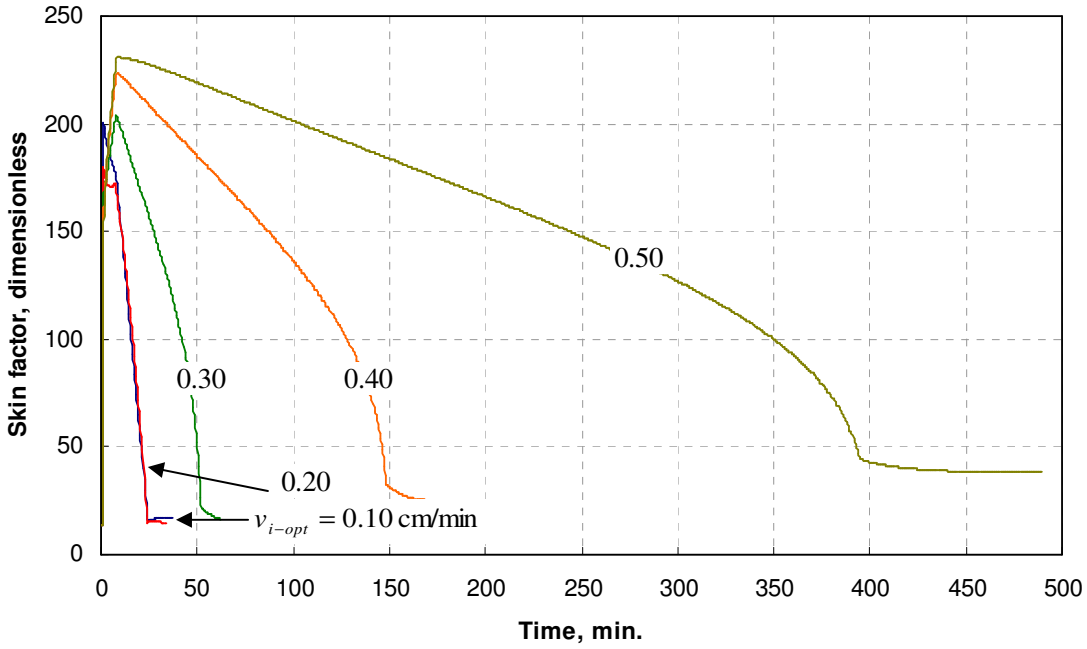

Fig. 5.13—A comparison of apparent skin factor profile among different optimal interstitial velocities.

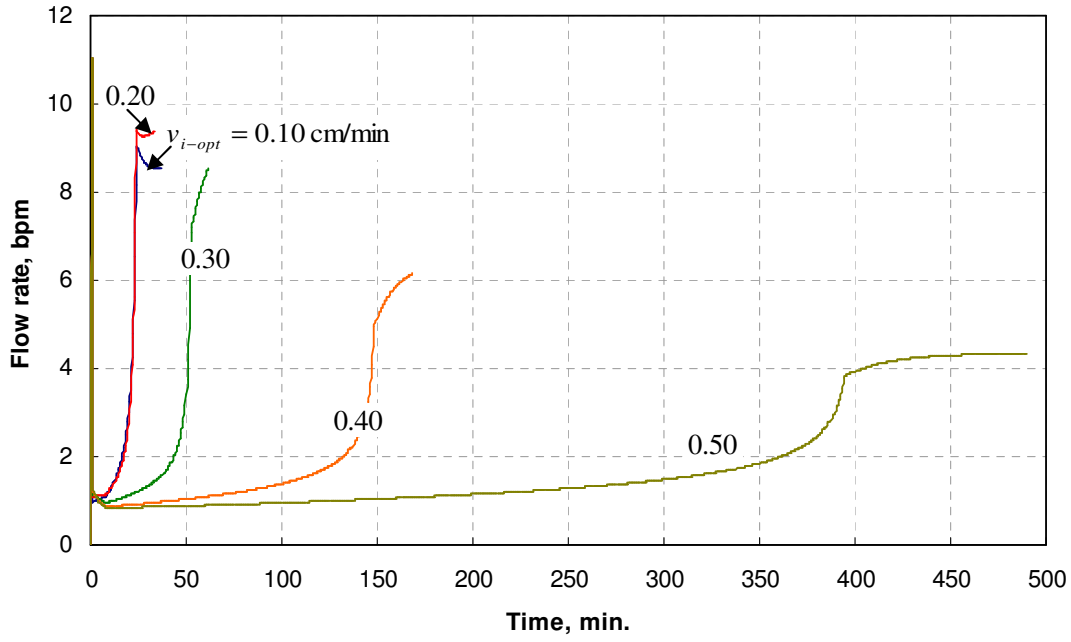

Fig. 5.14—A comparison of flow rate profile among different optimal interstitial velocities.

5.2 Multilayer Case

According to Fadale et al. (2000), the remarkable contrast of viscosity between acid solution and gas causes some viscous diversion to occur, and the viscous diversion is not very effective in re-distributing flow when the layer permeabilities differ significantly. In this section, we study this diversion effect. The data in this study are presented in **Tables 5.2** and **5.3**.

Table 5.2—Layers' data.

Layer No.	Thicknes (ft)	Permeability (md)	Damage permeability (md)	Porosity
1	100	2	1	0.25
2	100	6	1	0.25
3	10	1,000	1	0.25
4	150	4	1	0.25

Table 5.3—Data for multilayer case.

Reservoir data	
Formation temperature, ^{o}F	220
Apparent molecular weight	21.75
Critical gas saturation	0.10
Connate water saturation	0.20
Endpoint relative permeability to gas	0.90
Optimal pore volumes to break through	1.5
Optimal interstitial velocity, cm/min	0.6
Acid data	
Endpoint relative permeability to acid	0.50
Injection rate, bpm	2.0
Specific gravity of acid	1.1
Acid viscosity, cp	0.65
Wellbore data	
Well radius, ft	0.328
Slant angle, degrees	15
Tubing inner diameter, inches	4.5
Casing inner diameter, inches	6.184
Competion type	Openhole

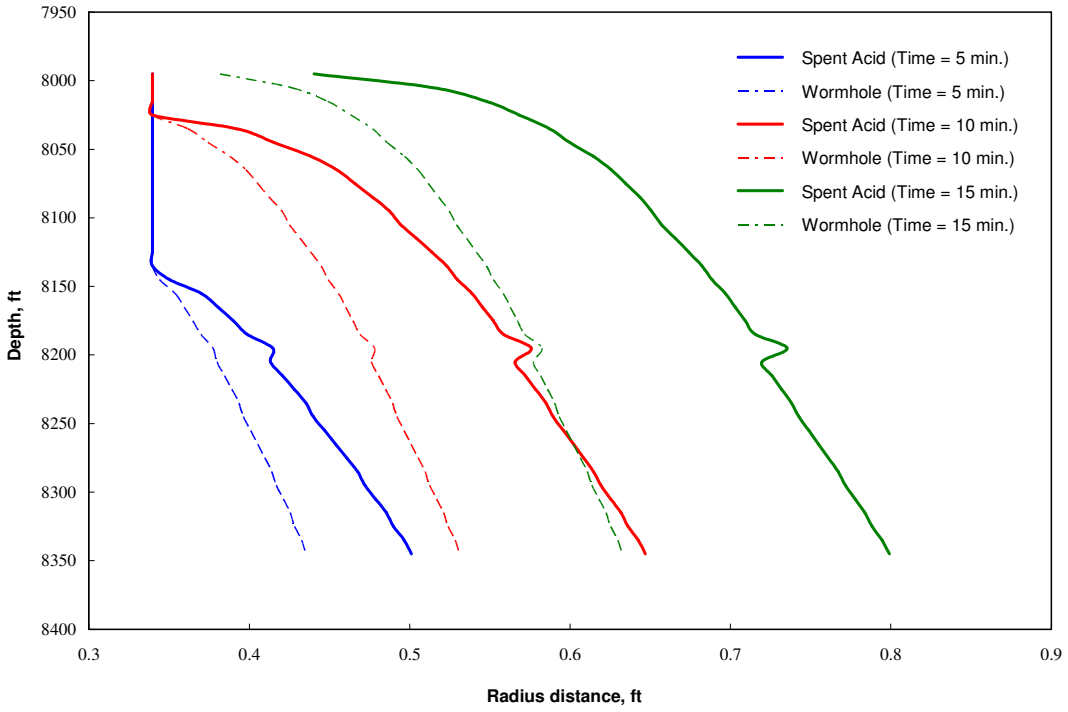

Fig. 5.15—Wormhole's and spent acid's fronts before wormhole breaks through.

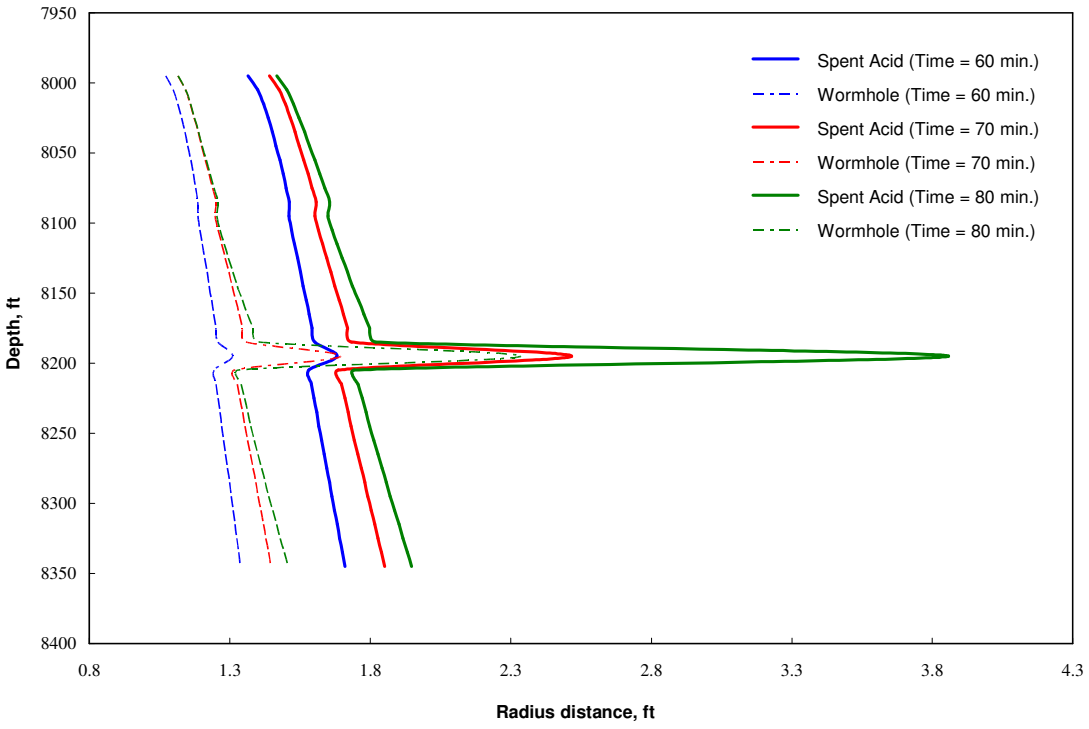

Fig. 5.16—Wormhole's and spent acid's fronts after wormhole breaks through.

Fig. 5.15 shows the wormhole's and spent acid's fronts before wormhole breaks through. Compared to a typical acid distribution in oil wells, the acid in layer 3 whose permeability is 1 darcy penetrates shallowly. As discussed in the previous section, original permeability does not affect the acid penetration so much. This is the diversion effect of mobility skin effect with combination of damage skin.

What will happen after wormhole breaks through? **Fig. 5.16** shows the result. Once wormhole goes through the damage region, the acid tends to flow into the higher-permeability zone. Hence, after wormhole breaks through, it is very hard to treat the lower-permeability zones. Because the lower-permeability zones also have their mobility skin effect, the situation is much worse than acidizing in oil wells. To treat the lower-permeability zones, some diverting method is needed.

6. CONCLUSIONS AND RECOMMENDATIONS

6.1 Conclusions

Shukla's experimental results (2002) have been analyzed successfully. The analysis has showed that the differential pressure in a gas saturated core does not linearly drop during acidizing. Rather than that, differential pressure can increase and the increase can be explained by the mobility difference between acid solution and gas.

On the basis of the analysis, a new apparent skin factor model has been developed. A placement model for matrix acidizing of vertically extensive, multilayer gas reservoirs has been developed with the model. With this model, it was found that:

- Before the wormhole in a higher-permeability zone breaks through, the combination of mobility and damage skin effect in the zone is a function of diverter.
- After the wormhole in a higher-permeability zone breaks through, the combination of mobility and damage skin effect in the other zones has a negative effect on acid diversion.

6.2 Recommendations

We analyzed Shukla's experimental results and showed that the change of differential pressure can be explained by the mobility difference between acid solution and gas. However, we did not construct how to get the speed of wormhole growth. If we

understand what happens after spent acid's front gets the outlet of the core, then we might be able to construct a wormholing model and a spent acid model for gas wells like Buijese and Glasbergen model. One of the biggest problem is to find out in what conditions there is enough spent acid ahead of the wormhole region to have mobility skin effect. It will be needed to carry out so many experiments to get some trends. Perhaps, that is still not enough. As discussed in section 3.6, the combination of damage and mobility skin effects has to be accounted for. Hence the criteria when spent acid causes big enough mobility skin effect may not be able to apply to the field case.

Also, the combination of mobility, damage, and completion skin effects needs to be studied. As many researchers noticed, the combination is not linear.

As to the wellbore flow, we must study the effects of gravity segregation and gas condensate in a wellbore.

In addition, it is needed to study diversion. Although mobility skin effect in higher-permeability zones diverts acid solution into lower permeability zone, once the wormhole in a higher-permeability zone breaks through, the effect does not work any more. Hence in the same way as matrix acidizing in oil wells, it is needed to construct a diversion model.

NOMENCLATURE

Symbol		Description
A	=	cross-sectional area to flow, L^2, ft^2
A'	=	cross-sectional area perpendicular to z-direction, L^2, ft^2
A_{eff}	=	effective cross-sectional area, L^2, ft^2
B	=	formation volume factor, resbbl/STB
c_t	=	total compressibility,Lt^2/m, psi^{-1}
D	=	pipe diameter, L, in.
f_{acid}	=	acid fractional flow, fraction
f_f	=	Fanning friction factor, dimensionless
h	=	thickness, L, ft
g	=	acceleration of gravity, L/t^2, ft/sec^2 [m/sec^2]
k	=	permeability, L^2, md
k_d	=	damage permeability, L^2, md
k_H	=	horizontal permeability, L^2, md
k_{rj}	=	relative permeability to phase j, dimensionless
k°_{rj}	=	endpoint relative permeability to phase j, dimensionless
k_V	=	vertical permeability, L^2, md
L_{core}	=	core length, L, ft [in.]
L_{spent}	=	length of spent acid penetration, L, ft
L_{wh}	=	length of wormhole penetration, L, ft

L^*_{wh} = length of wormhole penetration when spent acid breaks through, L, ft

M = mobility ratio, dimensionless

p = pressure, m/Lt^2, psi

p_D = dimensionless pressure, dimensionless

p_i = initial reservoir pressure, m/Lt^2, psi

PV = pore volumes, dimensionless

PV_{bt} = pore volumes to breakthrough, dimensionless

$PV_{bt\text{-}opt}$ = optimal pore volumes to breakthrough, dimensionless

q = flow rate, L^3/t, bbl/min

q_{inj} = injection rate, L^3/t, bbl/min

q_w = wellbore flow rate, L^3/t, bbl/min

q_{sR} = specific flow rate, L^2/t, bbl/(min-ft)

r = radius, ft

r_{spent} = spent acid penetration in radial geometry, L, ft

r_w = wellbore radius, ft

r_{wh} = wormhole penetration in radial geometry, L, ft

s = skin factor, dimensionless

s_{app} = apparent skin factor, dimensionless

s_d = damage skin factor, dimensionless

s_{vis} = viscous skin factor, dimensionless

t = time, t, days [minutes]

t_D = dimensionless time, dimensionless

u = velocity, L/t, ft/min

V_i = interstitial velocity of fluid, L/t, ft/min

$V_{i\text{-}opt}$ = optimal interstitial velocity, L/t, ft/min

V_{wh} = interstitial velocity of wormhole front, L/t, ft/min

W_{eff} = constant in wormhole model, $(L/t)^{1/3}$, $(m/s)^{1/3}$ $[(ft/min)^{1/3}]$

W_B = constant in wormhole model, $(L/t)^{-2}$, $(m/s)^{-2}$ $[(ft/min)^{-2}]$

z = elevation, L, ft

Z = gas compressibility (gas deviation factor), dimensionless

Greek

α_{spent} = Velocity at spent acid front, L, ft/PV

α_{wh} = Velocity at wormhole front, L, ft/PV

γ_a = Acid specific gravity, dimensionless

θ = slant angle, degrees [rad]

μ_j = viscosity of phase j, m/Lt, cp

ρ = density, m/L^3, lb_m/ft^3

ϕ = porosity, fraction

Δ = as a prefix for difference

Subscript

a = acid

c = constant

core = core

D	=	dimensionless
g	=	gas
i	=	initial
inj	=	injection
int	=	interface
max	=	maximum
spent	=	spent acid
w	=	wellbore
wh	=	wormhole

Superscript

◦	=	endpoint

REFERENCES

1. Besson, J. Performance of Slanted and Horizontal Wells on an Anisotropic Medium. Paper SPE 20965 presented at the 1990 European Petroleum Conference, Hague, The Netherlands, 21-24 October.
2. Brownscombe, E.R., and Collins, F. Pressure Distribution in Unsaturated Oil Reservoirs. *Trans. AIME*. **189**, 371-372. SPE-950371-G.
3. Buijse, M. and Glasbergen, G. A Semiempirical Model to Calculate Wormhole Growth in Carbonate Acidizing. Paper SPE 96892 presented at the 2005 Annual Technical Conference and Exhibition, Dallas, Texas, 9-12 October.3
4. Cinco-Ley, H., Miller, F.G., Ramey Jr., H.J. 1975. Unsteady-state Pressure Distribution Crated by a Directionally Drilled Well. *JPT* **27** (11): 1392-1400. SPE-5131-PA.
5. Conway, M. StimLab Acid Consortium Report, May 1997.
6. Eckerfield, L.D., Zhu, D., Hill, A.D., and Robert, J.A. 2000. Fluid Placement Model for Horizontal-Well Stimulation. *SPEDC* **15** (3): 185-190. SPE-65408-PA.
7. Fadale, O., Zhu, D., and Hill, A.D. Matrix Acidizing in Gas Wells. Paper SPE 59771 presented at the 2000 SPECERI Gas Technology Symposium, Calgary, Canada, 3-5 April.
8. Gdanski, R. Recent Advances in Carbonate Stimulation. Paper IPCT 10693 presented at the 2005 International Petroleum Technology Conference, Doha, Qatar, 21-23 November.

9. Hawkins Jr., M.F. 1956. A Note on the Skin Effect. *JPT* **8** (12):65-66. SPE-732-G.

10. Hill, A.D. and Galloway, P.J. 1984. Laboratory and Theoretical Modeling of Diverting Agent Behavior. *JPT* **36** (7): 1157-1163. SPE-11576-PA.

11. Hill, A.D. and Rossen, W.R. Fluid Placement and Diversion in Matrix-Acidizing. Paper SPE 27982 presented at the 1994 University of Tulsa Centennil Petroleum Engineering, Tulsa, Oklahoma, 29-31 August.

12. Hill, A.D. and Zhu, D. 1996. Real-Time Monitoring of Matrix Acidizing Including the Effects of Diverting Agents. *SPEPF* **11** (2): 95-101. SPE-28548-PA.

13. Jones, A.T. and Davies, D.R. Quantifying Acid Placement: The Key to Understanding Damage Removal in Horizontal Wells. Paper SPE 31146 presented at the 1996 SPE International Symposium on Formation Damage Control, Lafayette, Louisiana, 14-15 February.

14. Mishra, V. 2007. A Model for Matrix Acidizing of Long Horizontal Well in Carbonate Reservoirs. Master's thesis. Texas A&M University, College Station, Texas.

15. Mishra, V., Zhu, D., Hill, A.D., and Furui, K. An Acid-Placement Model for Long Horizontal Wells in Carbonate Reservoirs. Paper SPE 107780 presented at the 2007 European Formation Damage Conference, Scheveningen, The Netherlands, 30 May-1 June.

16. Rogers, E.J., Economides, M.J. The Skin Due to Slant of Deviated Wells in Permeability-Anisotropic Reservoirs. Paper SPE 37068 presented at the 1996 International Conference on Horizontal Well Technology, Calgary, Alberta, Canada, 18-20 November.
17. Seibt, D., Vogel, E., Bich, E., Buttig, D., and Hassel, E. 2006. Viscosity Measurements on Nitrogen. *Journal of Chemical and Engineering Data*. **51** (2): 526-533.
18. Suneet, S. 2002. Gas Assisted Acidizing of Carbonate Reservoirs. Master's thesis. The University of Texas at Austin, Austin, Texas.
19. Tardy, P.M.J., Lecerf, B., and Christanti, Y. Paper SPE 107854 presented at the 2007 European Formation Damage Conference, Scheveningen, The Netherlands, 30 May-1 June.
20. Zhu, D., Hill, A.D., and da Motta, E.P. On-site Evaluation of Acidizing Treatment of a Gas Reservoir. Paper 39421 presented at the 1998 SPE International Symposium on Formation Damage Control, Lafayette, Louisiana, 18-19 February.

VITA

Name: Manabu Nozaki

Address: 4-8-14 Kamikido, Higashi-Ku,
Niigata, Niigata,
950-0891, Japan

Education: B.E., Resources and Environmental Engineering, Waseda University, 2006

This thesis was typed by the author.